Dual role for DOCK7 in tangential migration of interneuron precursors in the postnatal forebrain

Shinichi Nakamuta,[1]* Yu-Ting Yang,[1]* Chia-Lin Wang,[1]* Nicholas B. Gallo,[1,2] Jia-Ray Yu,[1] Yilin Tai,[1] and Linda Van Aelst[1]

[1]Cold Spring Harbor Laboratory, Cold Spring Harbor, NY
[2]Department of Neurobiology and Behavior, Stony Brook University, Stony Brook, NY

Throughout life, stem cells in the ventricular–subventricular zone generate neuroblasts that migrate via the rostral migratory stream (RMS) to the olfactory bulb, where they differentiate into local interneurons. Although progress has been made toward identifying extracellular factors that guide the migration of these cells, little is known about the intracellular mechanisms that govern the dynamic reshaping of the neuroblasts' morphology required for their migration along the RMS. In this study, we identify DOCK7, a member of the DOCK180-family, as a molecule essential for tangential neuroblast migration in the postnatal mouse forebrain. DOCK7 regulates the migration of these cells by controlling both leading process (LP) extension and somal translocation via distinct pathways. It controls LP stability/growth via a Rac-dependent pathway, likely by modulating microtubule networks while also regulating F-actin remodeling at the cell rear to promote somal translocation via a previously unrecognized myosin phosphatase–RhoA–interacting protein-dependent pathway. The coordinated action of both pathways is required to ensure efficient neuroblast migration along the RMS.

Introduction

Migration of neuronal precursors from their place of birth to their final location in the central nervous system is crucial not only for the establishment but also for the maintenance and modification of neural circuitry (Hatten, 2002; Marín and Rubenstein, 2003; Ghashghaei et al., 2007; Evsyukova et al., 2013). Although the bulk of neuronal precursor generation and migration in the mammalian brain occurs during the embryonic period, these processes do persist in restricted areas of the postnatal/adult brain (Ghashghaei et al., 2007; Kempermann et al., 2015; Lim and Alvarez-Buylla, 2016). Among them is the ventricular–subventricular zone (V-SVZ), which in rodents is located along the walls of the brain lateral ventricles (Alvarez-Buylla and Garcia-Verdugo, 2002). In the V-SVZ, each day, neural stem cells give rise to thousands of interneuron precursors, termed V-SVZ neuroblasts, that migrate tangentially over a long distance to the olfactory bulb (OB), where they differentiate into various subtypes of local circuit interneurons (Luskin, 1993; Lois and Alvarez-Buylla, 1994; Petreanu and Alvarez-Buylla, 2002; Belluzzi et al., 2003; Carleton et al., 2003; Fuentealba et al., 2012; Merkle et al., 2014). This continual influx of new neurons enables constant modification of OB neural circuits, a property vital for olfactory information processing (Arenkiel, 2010; Belvindrah et al., 2011; Lazarini and Lledo, 2011; Sawada and Sawamoto, 2013; Obernier et al., 2014; Sakamoto et al., 2014; Sailor et al., 2017).

The tangential migration of neuroblasts from the V-SVZ to the OB in the postnatal/adult forebrain is remarkable not only for the long distance they migrate (up to 3–8 mm in rodents) but also for the highly directed nature of the migration (Luskin, 1993; Lois and Alvarez-Buylla, 1994). After their generation and initial differentiation in the V-SVZ, neuroblasts organize into a network of interconnected chains surrounded by astroglial tubes to migrate in a restricted and highly oriented path known as the rostral migratory stream (RMS; Doetsch and Alvarez-Buylla, 1996; Lois et al., 1996; Wichterle et al., 1997; Kaneko et al., 2010; James et al., 2011; Wang et al., 2011). Interestingly, in the RMS, neuroblasts use each other as migratory substrate as opposed to the radial glial-guided or axonal-guided modes of neuronal migration identified in the developing brain (Wichterle et al., 1997; Nam et al., 2007). RMS neuroblasts crawl along each other as they move forward toward the OB and do so through a repetitive cycle composed of leading process (LP) elongation and saltatory movement of the soma and nucleus (Schaar and McConnell, 2005; Ghashghaei et al., 2007;

*S. Nakamuta, Y.-T. Yang, and C.-L. Wang contributed equally to this paper.

Correspondence to Linda Van Aelst: vanaelst@cshl.edu

Y.-T. Yang's and C.-L. Wang's present address is Mirimus Inc, Brooklyn, NY.

J.-R. Yu's present address is New York University School of Medicine, New York, NY.

Abbreviations used: DCX, doublecortin; GEF, guanine nucleotide exchange factor; INM, interkinetic nuclear migration; LP, leading process; MLCP, myosin light chain phosphatase; MT, microtubule; OB, olfactory bulb; RGC, radial glial progenitor cell; RIPA, radioimmunoprecipitation assay; RMS, rostral migratory stream; ROCK, Rho-kinase; V-SVZ, ventricular–subventricular zone; YTH, yeast two-hybrid.

The Rockefeller University Press
J. Cell Biol. Vol. 216 No. 12 4313–4330
https://doi.org/10.1083/jcb.201704157

Métin et al., 2008; Trivedi and Solecki, 2011). Namely, they first extend a dynamic LP to sample the surrounding environment, whereas the soma and nucleus remain largely stationary. Then, after the LP is consolidated and commits to a single direction, the nucleus, along with the soma, translocates forward in a two-step process called nucleokinesis. The latter begins with the centrosome moving forward to a "swelling" that is transiently formed in the proximal part of the extending LP, followed by the movement of the nucleus and soma toward the centrosome. This cycle of intricately coupled LP extension and nucleokinesis is repeated many times as the neuroblast propels itself forward.

Although the cellular/molecular basis of radial glial-guided neuronal migration has been extensively studied (Fishell and Hatten, 1991; Komuro and Rakic, 1998; Solecki et al., 2004, 2009; Tanaka et al., 2004; Tsai et al., 2007; He et al., 2010; Marín et al., 2010; Govek et al., 2011; Cooper, 2013; Trivedi et al., 2017), how tangentially migrating V-SVZ neuroblasts control and coordinate LP extension and nucleokinesis to accomplish efficient migration is less well understood. Although live-cell imaging studies have begun to unveil the requirements of microtubule (MT) and actomyosin cytoskeletal elements during the distinct phases of V-SVZ neuroblast migration (Schaar and McConnell, 2005; Shinohara et al., 2012; Ota et al., 2014), still little is known about the intrinsic factors that impinge on the neuroblasts' cytoskeleton to govern LP extension and somal/nuclear translocation. Only a relatively small number of molecules have so far been reported to control one of these two phases of neuroblast migration in the postnatal/adult forebrain (Anton et al., 2004; Koizumi et al., 2006; Hirota et al., 2007; Leong et al., 2011; Mejia-Gervacio et al., 2012; Shinohara et al., 2012; Sonego et al., 2015). Among them, Cdk5 and its substrate doublecortin (DCX), an MT-regulatory protein, have been implicated in the growth and maintenance of the V-SVZ neuroblasts' LP (Kappeler et al., 2006; Koizumi et al., 2006; Hirota et al., 2007), whereas the Rho-regulated actin nucleators mDia1 and mDia3, in cooperation with Rho-kinase (ROCK), have been shown to regulate nucleokinesis (Shinohara et al., 2012). Of note, neuroblasts lacking mDia1/3 proteins still display a normal LP (Shinohara et al., 2012), and although DCX-deficient neuroblasts also exhibit nuclear translocation defects, the latter could be secondary to the LP defects (Koizumi et al., 2006). Despite the need for the coupling of LP extension and nucleokinesis to ensure efficient migration of V-SVZ neuroblasts, currently there is little information on how this occurs at a molecular level.

Driven by our previous research unveiling a key role for DOCK7, a member of the DOCK180 family of atypical Rac/Cdc42 guanine nucleotide exchange factors (GEFs; Gadea and Blangy, 2014; Laurin and Côté, 2014), in the genesis of new neurons during embryonic cortical development (Yang et al., 2012), we set out to explore the potential role of DOCK7 in postnatal/adult neurogenesis. In this study, we show that DOCK7 is expressed in OB interneuron precursors in the V-SVZ–RMS regions of the postnatal/adult mouse forebrain, and we demonstrate that DOCK7 is critical for the tangential migration of V-SVZ neuroblasts to the OB but not for the generation or proliferation of these cells. Interestingly, using a molecular replacement strategy combined with live-cell imaging, we uncover that DOCK7 governs the migration of V-SVZ neuroblasts by controlling both LP extension and nucleokinesis. Moreover, we find that DOCK7 controls these two processes by acting on distinct pathways. Namely, it controls LP stability/growth via a Rac-dependent pathway, likely by stabilizing MTs, whereas it regulates somal/nuclear translocation by modulating F-actin dynamics at the cell rear via a previously unrecognized myosin phosphatase–RhoA–interacting protein ($p116^{Rip}$)-dependent pathway. Thus, our study identifies DOCK7 as a novel molecule that regulates both phases of V-SVZ neuroblast migration. Thereby, it not only offers new insight into DOCK7 function, but it also provides a greater understanding of the mechanisms that govern the multifaceted steps undertaken by tangentially migrating V-SVZ neuroblasts in the postnatal forebrain.

Results

DOCK7 expression along the V-SVZ–RMS–OB migratory pathway

To assess DOCK7's role in postnatal V-SVZ/OB neurogenesis, we began by examining its expression patterns in the V-SVZ and RMS/OB regions of the postnatal/adult mouse forebrain. To this end, we performed Western blot analysis of DOCK7 using lysates prepared from the V-SVZ, RMS, and OB regions of postnatal day 10 (P10) and adult (P45) mouse brains. We found that DOCK7 was prominently expressed in the V-SVZ and RMS/OB of both P10 and P45 mice (Fig. S1, A and B). In addition, we performed immunohistochemistry on coronal cryosections of P10 and P45 mouse brains (Fig. 1, A–C; and Fig. S1, C–E). In line with our Western blot data, DOCK7 immunostaining was observed in the V-SVZ and along the RMS to the OB of both P10 and P45 mouse forebrains (Fig. 1, B and C; and Fig. S1, D and E). To determine which cell types in the V-SVZ/RMS neurogenic regions express DOCK7, we coimmunostained brain sections with antibodies against GFAP, MASH1, or DCX, which label astrocytelike stem cells, transit-amplifying progenitor cells (TAPs), and neuroblasts, respectively. In the V-SVZ, DOCK7 immunoreactivity was detected in most of the GFAP-positive astrocytelike stem cells, MASH1-positive TAPs, and DCX-positive neuroblasts (Fig. 1, B and C; and Fig. S1, D and E), suggesting the presence of DOCK7 in all three cell types. In accordance, when slices were costained with an antibody against nestin, which labels subpopulations of all three cell types (Kim et al., 2009; Codega et al., 2014), overlapping staining of DOCK7 with nestin was seen in the majority of the cells (Figs. 1 C and S1 E). Notably, upon zooming in on the RMS, we saw prominent colocalization of DOCK7 with DCX over the entire region of the RMS (Figs. 1 B and S1 D), indicating that DOCK7 is expressed by the migrating neuroblast subpopulation derived from the V-SVZ. The presence of DOCK7 in V-SVZ–derived neuroblasts was further confirmed by immunofluorescent stainings of neuroblasts dissociated from postnatal V-SVZ tissue (Fig. 1 D). In these cells, DOCK7 signal was detected in the cytoplasm of the cell body and along the LP, where it overlapped with that of βIII-tubulin, a neuronal marker that labels MTs. Combined, these data unveil the presence of DOCK7 along the postnatal V-SVZ–RMS–OB pathway, where it is prominently expressed in V-SVZ–derived migratory neuroblasts.

DOCK7 depletion impairs the migration of V-SVZ neuroblasts en route to the OB

The prominent expression of DOCK7 in neuroblasts along the V-SVZ–RMS–OB pathway prompted us to examine whether DOCK7 is involved in the tangential migration of these cells

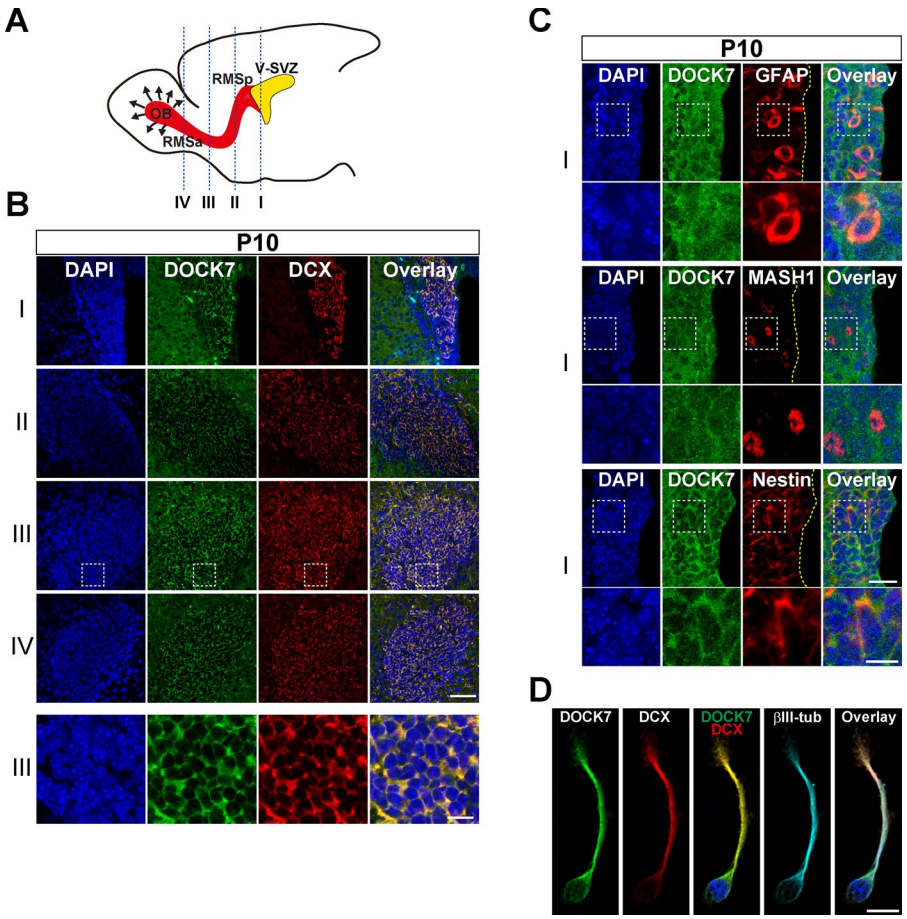

Figure 1. **Expression of DOCK7 in the postnatal mouse forebrain.** (A) A cartoon representation of the V-SVZ–RMS–OB pathway. (B) Coronal sections of forebrains of P10 mice at positions indicated in the cartoon in A immunostained with antibodies to DOCK7 and DCX and counterstained with DAPI. Boxed regions in III are enlarged and shown at the bottom. Bars: (top) 50 µm; (bottom) 10 µm. (C) Coronal sections of the V-SVZ region of P10 mice immunostained with antibodies to DOCK7 and GFAP, MASH1, or nestin and counterstained with DAPI. Boxed regions are enlarged and shown at the bottom. The yellow dashed line indicates the boundary region between the V-SVZ and the lateral ventricle. Bars: (top) 25 µm; (bottom) 10 µm. (D) Localization of DOCK7 in cultured V-SVZ–derived neuroblasts. Neuroblasts dissociated from V-SVZ tissue of P1–3 mice were fixed at 30 h in vitro, followed by immunostaining with indicated antibodies and counterstaining with DAPI. Bar, 10 µm.

en route to the OB. To approach this, we combined in vivo electroporation methodology (Fig. 2 A; Chesler et al., 2008; Sonego et al., 2013) with RNAi to knock down endogenous DOCK7 protein levels in neuroblasts derived from stem/progenitor cells located in the V-SVZ of neonatal mice. For RNAi, we used previously described vectors that express an shRNA targeting the DOCK7 protein coding sequence (Dock7#1) or the 3′ UTR (Dock7#2) of mouse *DOCK7* mRNA or a control scrambled (scr#1) shRNA (Watabe-Uchida et al., 2006; Yang et al., 2012).

Each of these vectors was introduced together with an EGFP-encoding plasmid into the lateral ventricles of P3 mice and transduced into neural stem cells by electroporation. 7 d postelectroporation (dpe), at P10, sagittal brain slices were prepared and analyzed by spinning-disk confocal microscopy. As expected, in the scr#1 shRNA group, EGFP-positive cells were noted along the RMS, with the majority of them residing in the anterior part of the RMS (RMSa) and in the OB (Fig. 2, B and C), indicating that many of the neuroblasts had migrated into this structure. In contrast, in both the Dock7#1 and Dock7#2 shRNA groups, EGFP-positive cells accumulated in high numbers in the posterior part of the RMS (RMSp) and were much fewer in number in the OB (Fig. 2, B and C), implying that the neuroblasts were impaired in their migration toward the OB. Of note, when the mouse pups were electroporated at P3 with the Dock7#2 shRNA-expressing vector with brain slices analyzed 14 d later at P17, perturbations in the migration of neuroblasts were still observed (Fig. 2 D). Interestingly, closer scrutiny of the neuroblasts' morphology in the RMS revealed that a considerable fraction of the Dock7 shRNA-expressing cells exhibited an aberrant LP (Fig. 2 E). The length of the LP was significantly shorter than that of the control neuroblasts, and many of the cells displayed branched LPs (Fig. 2, E and F), suggesting a role for DOCK7 in LP growth/stability (see next section).

To confirm that the observed phenotypes were caused by specific knockdown of DOCK7, we performed rescue experiments using DOCK7 cDNA that lacked the 3′ UTR and was therefore resistant to Dock7#2 shRNA-mediated RNA interference. We observed that coexpression of RNAi-resistant DOCK7 cDNA with Dock7#2 shRNA completely rescued the RNAi-induced phenotypes (Fig. 2, B, C, E, and F), demonstrating that the effects of DOCK7 RNAi were specific. We also found that DOCK7 knockdown did not affect stem/progenitor cell proliferation nor neuroblast generation (Fig. S1, F–H; and not depicted), indicating that the reduction in the number of neuroblasts migrating toward the OB was not a result of changes in neuroblast production. Collectively, these data support a critical role for DOCK7 in the migration, but not generation, of V-SVZ–derived neuroblasts along the RMS en route to the OB. Of note, our finding that DOCK7 knockdown does not appreciably affect the generation of neuroblasts in the postnatal forebrain may appear at odds with our previous study in the embryonic neocortex demonstrating a requirement for DOCK7 in the genesis of new neurons from radial glial progenitor cells (RGCs; Yang et al., 2012). In the latter case, however, DOCK7 influences the genesis of neurons by controlling interkinetic nuclear migration (INM) of RGCs, a process where RGC nuclei undergo a cell cycle–dependent change in position along the apical–basal axis of the ventricular zone, with proliferative signals being high at the apical side and neurogenic signals at the basal side (Taverna and Huttner, 2010). To what extent, if at all, astrocytelike

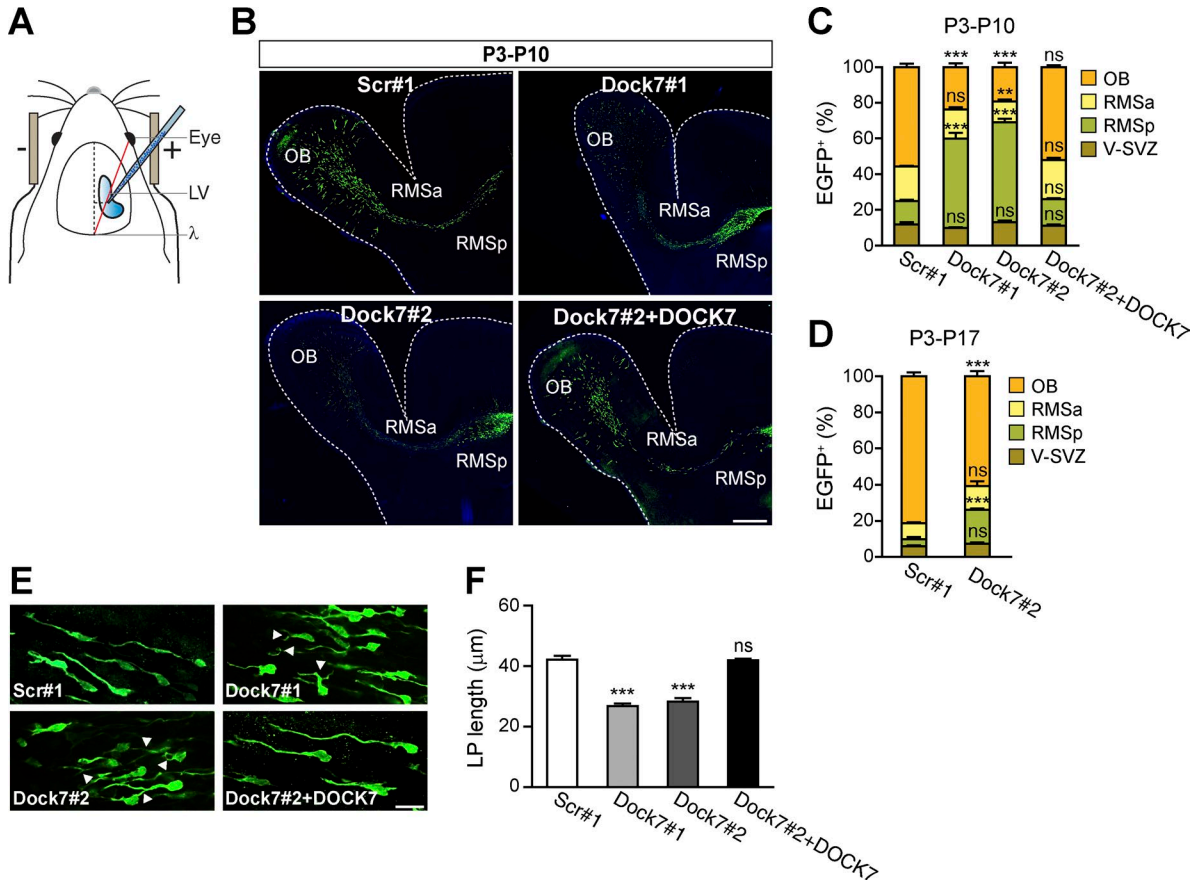

Figure 2. **DOCK7 function is required for the migration of neuroblasts along the RMS.** (A) Schematic drawing of postnatal in vivo electroporation. A virtual line (red) connecting the right eye to the craniometrical landmark λ serves as positional marker for plasmid injection into the lateral ventricle (LV). Lateral bars indicate position of electrodes. (B) Composite confocal images of forebrains of mice electroporated at P3 with plasmids expressing EGFP and nontargeting shRNA (scr#1), Dock7-targeting shRNAs (Dock7#1 and Dock7#2), or Dock7#2 shRNA together with DOCK7 cDNA (Dock7#2 + DOCK7) and sacrificed at P10 showing distribution of EGFP⁺ transfected cells along the V-SVZ–RMS–OB pathway. Slices were counterstained with DAPI. Dotted lines outline borders of sagittal slices. Bar, 500 µm. (C) Quantification of the distribution of EGFP⁺ transfected cells along the V-SVZ–RMS–OB pathway in the forebrains of mice electroporated at P3 and sacrificed at P10. *n* = 1,316–2,511 cells from at least three animals for each condition. (D) Quantification of the distribution of EGFP⁺ transfected cells along the V-SVZ–RMS–OB pathway in the forebrains of mice electroporated at P3 and sacrificed at P17. *n* = 2,379–2,462 cells from at least three animals for each condition. (E) Enlarged images of neuroblasts in RMSp regions of mice electroporated with indicated constructs at P3 and sacrificed at P10. Arrowheads indicate branching of LP. Bar, 20 µm. (F) Quantification of the length of the LP of neuroblasts in the RMS of mice electroporated with indicated constructs at P3 and sacrificed at P10. *n* = 91–680 cells from at least three animals for each condition. Data are shown as means ± SEM. **, P < 0.01; ***, P < 0.001; ns, P > 0.05 compared with scr#1; one-way ANOVA with Dunnett's post hoc test (C and F) or Student's *t* test (D).

stem cells in the postnatal (>P10)/adult V-SVZ undergo INM remains unclear (Tramontin et al., 2003), and to the best of our knowledge no study to date has implicated INM in the genesis of V-SVZ neuroblasts. Thus, the role DOCK7 plays in a particular cell type and/or cellular process is likely context dependent.

Altered dynamics of V-SVZ neuroblast migration upon depletion of DOCK7

To better understand the dynamics of the migration defect seen in DOCK7-depleted neuroblasts, we performed live imaging experiments to track the migration of control and DOCK7 knockdown neuroblasts. To this end, P2–3 mouse pups were electroporated with vectors expressing control scr#1 or Dock7#2 shRNA, together with a tdTomato-expressing plasmid, and organotypic forebrain slices were prepared 5 d later at P7–8. Slices harboring tdTomato-labeled cells in the RMS were imaged at 4-min intervals over a period of 4 h.

Tracking analyses revealed that Dock7#2 shRNA-expressing neuroblasts were overall less directed in their movement and displayed reduced migration distance, displacement, and velocity as compared with control scr#1 shRNA-expressing neuroblasts (Fig. 3, A–D; and Videos 1 and 2). Notably, coexpression of RNAi-resistant DOCK7 with Dock7#2 shRNA was able to rescue the migratory defects induced by DOCK7 knockdown (Fig. 3, B–D; and Video 3). Interestingly, upon more closely monitoring the branching frequency of the neuroblasts' LP in our time-lapse videos, we observed that knockdown of DOCK7 markedly increased the frequency of branching events (defined as the appearance of secondary branches either from the primary process or from the cell body). Compared with scr#1 shRNA-expressing cells, the number of branching events was nearly doubled in Dock7#2 shRNA-expressing cells (Fig. 3, E and F), implying that DOCK7-depleted neuroblasts fail to suppress secondary branching and consolidate a single LP. Together, these findings substantiate the requirement of DOCK7 for the stabilization/growth of the LP and the efficient migration of V-SVZ neuroblasts along the RMS.

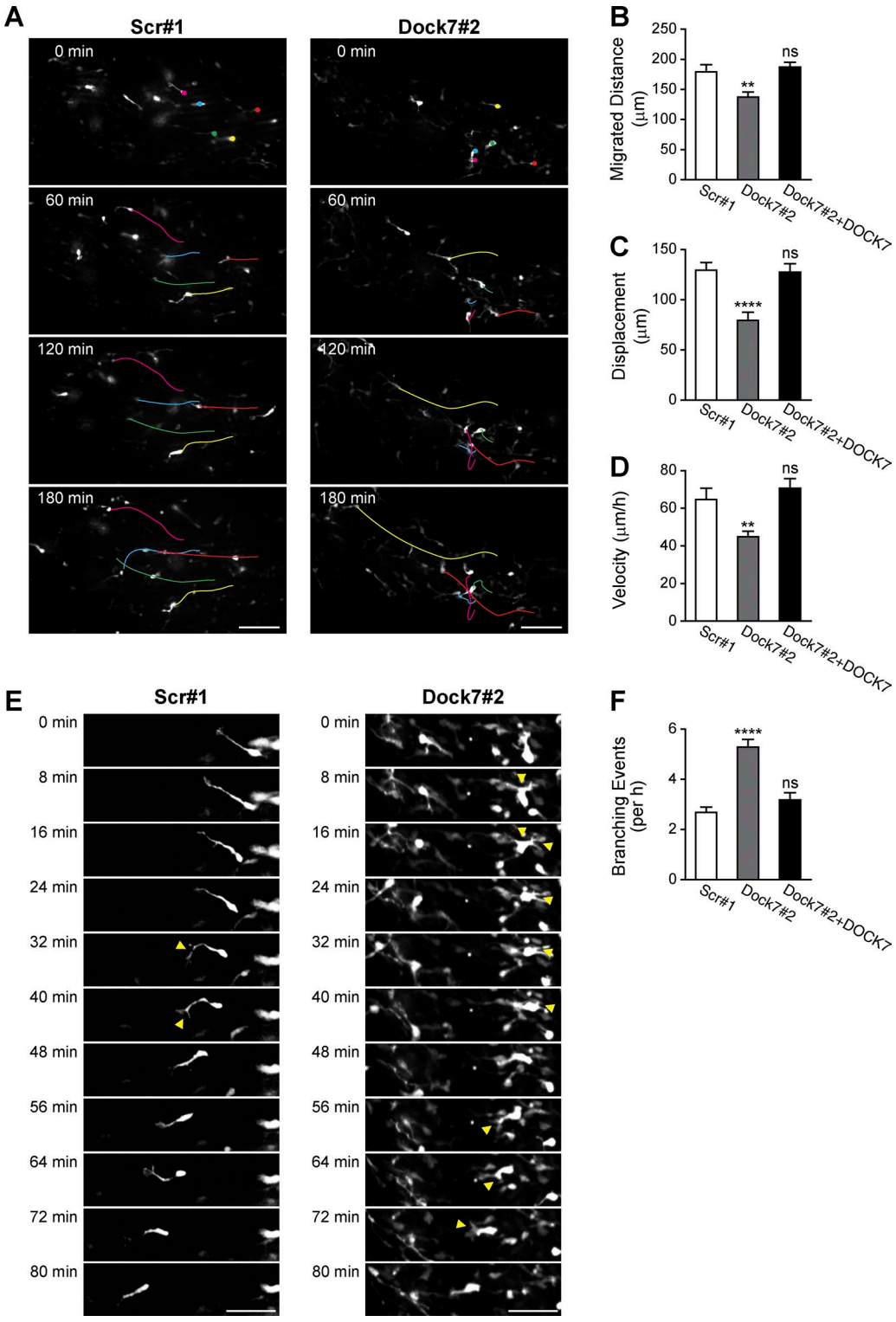

Figure 3. **Knockdown of DOCK7 affects the migration distance, displacement, speed, and LP branching frequency of migrating neuroblasts.** (A–F) P2–3 mouse pups were electroporated with plasmids expressing tdTomato and scr#1, Dock7#2 shRNA, or the rescue construct (Dock7#2 + DOCK7). After 5 d, acute sagittal brain slices were prepared, and tdTomato$^+$ transfected neuroblasts were imaged by spinning-disk confocal microscopy over a 4-h time period. (A) Time-lapse sequence of scr#1 or Dock7#2 shRNA-expressing cells migrating in the lower vertical arm of the RMSp. Five cells in each slice are labeled in the 0-min panel, and their tracks over time are indicated by lines of the same color. Bars, 70 µm. (B–D) Quantifications of the mean migrated distance (B), displacement (C), and velocity (D) of neuroblasts expressing indicated constructs. *n* = 50–61 cells from five to seven animals for each condition. (E) Examples of time-lapse series of scr#1 or Dock7#2 shRNA-expressing cells in the lower vertical arm of the RMSp (higher magnification). Arrowheads indicate branching of LP. Bars, 50 µm. (F) Quantification of the number of branching events per h for neuroblasts expressing indicated constructs. *n* = 50–61 cells from five to seven animals for each condition. Data are shown as means ± SEM. **, P < 0.01; ****, P < 0.0001; ns, P > 0.05 compared with scr#1; one-way ANOVA with Dunnett's post hoc test.

DOCK7 controls neuroblast migration via DHR2/Rac-dependent and DHR2/Rac-independent pathways

To gain insight into the molecular mechanism or mechanisms by which DOCK7 controls the migration of V-SVZ neuroblasts, we initiated rescue experiments with (a) DOCK7ΔDHR2 and DOCK7-V2022A mutants, which harbor a deletion and point mutation, respectively, in the catalytic DHR2 domain and are defective in Rac activation (Figs. 4 A and S2 A; Watabe-Uchida et al., 2006), and we also used (b) a DOCK7 deletion mutant (DOCK7ΔR2), which lacks the conserved DHR1 domain and adjacent C-terminally located amino acid residues comprising the transforming acidic coiled-coil containing protein 3 (TACC3)-binding domain (Fig. 4 A; Yang et al., 2012). Each of these mutants was coexpressed with Dock7#2 shRNA in neuroblasts in the V-SVZ of P3 pups, and the distribution of neuroblasts along the V-SVZ–RMS–OB pathway was analyzed 7 d postelectroporation. We found that DOCK7ΔDHR2 and DOCK7-V2022A failed to rescue the DOCK7 RNAi-induced defects in neuroblast migration, in contrast with DOCK7 (Fig. 4, B and C). These cells, similar to DOCK7 RNAi-expressing cells, accumulated in large numbers in the RMSp and displayed a shorter/aberrant LP (Fig. 4, B–D). Moreover, live-cell imaging experiments showed that neuroblasts coexpressing Dock7#2 shRNA and DOCK7ΔDHR2 had a lower mean speed, a reduction in distance migrated and displacement, and branched more frequently compared with cells coexpressing Dock7#2 shRNA and DOCK7 (Fig. 4, E–H; Fig. S2 B; and Videos 3 and 4). These data indicate that DOCK7's DHR2 domain and GEF activity toward Rac are essential for its role in LP stability/growth and V-SVZ neuroblast migration.

Intriguingly, we observed that the DOCK7ΔR2 mutant also failed to rescue the DOCK7 RNAi-induced defects in neuroblast migration, albeit these cells, in contrast to cells coexpressing Dock7#2 shRNA and DOCK7ΔDHR2, displayed an intact LP whose length was similar to that of control neuroblasts (Fig. 4, B–D). Of note, DOCK7 mutants lacking the R2 domain are still able to activate Rac (Watabe-Uchida et al., 2006; Yang et al., 2012). Live-cell imaging experiments corroborated that the migration of neuroblasts coexpressing Dock7#2 shRNA and DOCK7ΔR2 was impaired. Cells migrated more slowly, and the migration distance was significantly reduced (Fig. 4, E–G; and Video 5). Importantly, live-cell imaging also confirmed that the LP of these cells was overall intact. The cells exhibited a typical polarized LP, and, in contrast with cells coexpressing Dock7#2 shRNA and DOCK7ΔDHR2, they did not display increased branching frequency (Figs. 4 H and S2 B), thus implying that the R2-dependent pathway controls a step in neuroblast migration that is distinct from LP stability/growth. Combined, these results unveil that DOCK7 controls neuroblast migration by acting on both DHR2/Rac-dependent and R2-dependent pathways, each influencing distinct aspects of neuroblast migration.

DOCK7 interacts with p116^{Rip}

These findings demonstrate the requirement of a DHR2/Rac-dependent pathway in mediating DOCK7's effect on LP stability/growth, a pathway we previously showed to control axon elongation via the modulation of MT networks (Watabe-Uchida et al., 2006). An outstanding question, however, is what R2-dependent mechanism or mechanisms mediate DOCK7 function in V-SVZ neuroblasts. Although DOCK7 was shown to also interact with the MT-associated protein TACC3 to control INM and the genesis of neurons in the embryonic neocortex (Yang et al., 2012), we did not detect TACC3 expression in postnatal V-SVZ/RMS neurogenic regions (Fig. S2 C). This finding excludes TACC3 as a possible candidate for mediating the R2-dependent function of DOCK7 in V-SVZ neuroblasts and is in line with our observation that DOCK7 knockdown does not affect the generation of these cells. Hence, we decided to search for additional DOCK7 interaction partners. To this end, we used the yeast two-hybrid (YTH) approach to screen an adult mouse brain cDNA library with the DOCK7-R2 fragment as bait (Fig. 5 A). Interestingly, we found that six of the positive clones contained identical cDNAs encoding a C-terminal fragment of p116^{Rip} (Fig. 5, A and B). p116^{Rip}, also known as M-RIP, is an F-actin–binding protein that was originally identified as a binding partner of RhoA (Gebbink et al., 1997) and subsequently of the myosin-binding subunit of myosin light chain phosphatase (MLCP; Surks et al., 2003). The protein has since been implicated in the regulation of the actomyosin-based cytoskeleton in nonneuronal cells (Mulder et al., 2003, 2004; Surks et al., 2005; Riddick et al., 2008).

Before further validating the interaction between DOCK7 and p116^{Rip}, we first determined whether p116^{Rip} is expressed in neuroblasts in the postnatal forebrain. Immunohistochemistry for p116^{Rip} showed that the protein is indeed expressed in neuroblasts in the V-SVZ and along the RMS of P10 mouse forebrains (Fig. 5 C). We then verified the interaction between DOCK7 and p116^{Rip} by several approaches. First, we confirmed the YTH interaction by coimmunoprecipitation experiments using lysates from HEK293 cells expressing Flag-tagged DOCK7 and endogenous p116^{Rip} (Fig. 5 D). Second, we demonstrated the association between DOCK7 and p116^{Rip} by pulldown experiments using a GST-p116^{Rip} C-terminal fragment fusion protein (GST-p116^{Rip}-C). Beads loaded with GST-p116^{Rip}-C, but not GST alone, efficiently pulled down DOCK7 from lysates of P5 mouse forebrains (Fig. 5 E). Third, reciprocal coimmunoprecipitations of endogenous DOCK7 and p116^{Rip} proteins from mouse whole-brain extracts corroborated that the two proteins associate with each other in vivo (Fig. 5 F). Finally, immunofluorescence studies showed overlapping staining of DOCK7 with p116^{Rip} in neuroblasts in the RMS of P10 mouse forebrains (Fig. 5 G) as well as in neuroblasts dissociated from postnatal V-SVZ tissue (Fig. 5 H). Together, these data establish that DOCK7 and p116^{Rip} form a complex in V-SVZ–derived neuroblasts.

DOCK7 interaction with p116^{Rip} is crucial for V-SVZ neuroblast migration

Next, we investigated the importance of the DOCK7–p116^{Rip} interaction in V-SVZ neuroblast migration. To approach this, we first examined the function of endogenous p116^{Rip} by probing the effects of reduced p116^{Rip} expression on the migration of V-SVZ neuroblasts (Figs. 6 and S3). Vectors were generated that express shRNAs targeting three independent sequences within the translated region of p116^{Rip} (p116^{Rip}#1, p116^{Rip}#2, and p116^{Rip}#3). All three shRNAs substantially reduced p116^{Rip} expression in cortical neurons, whereas control shRNA (scr#2) had no effect (Fig. S3 A). Each of these vectors was then introduced together with an EGFP-encoding plasmid into the lateral ventricles of P3 mouse pups before in vivo electroporation, and 7 d later, sagittal brain slices were prepared, and the distribution of EGFP-labeled cells along the V-SVZ–RMS–OB pathway

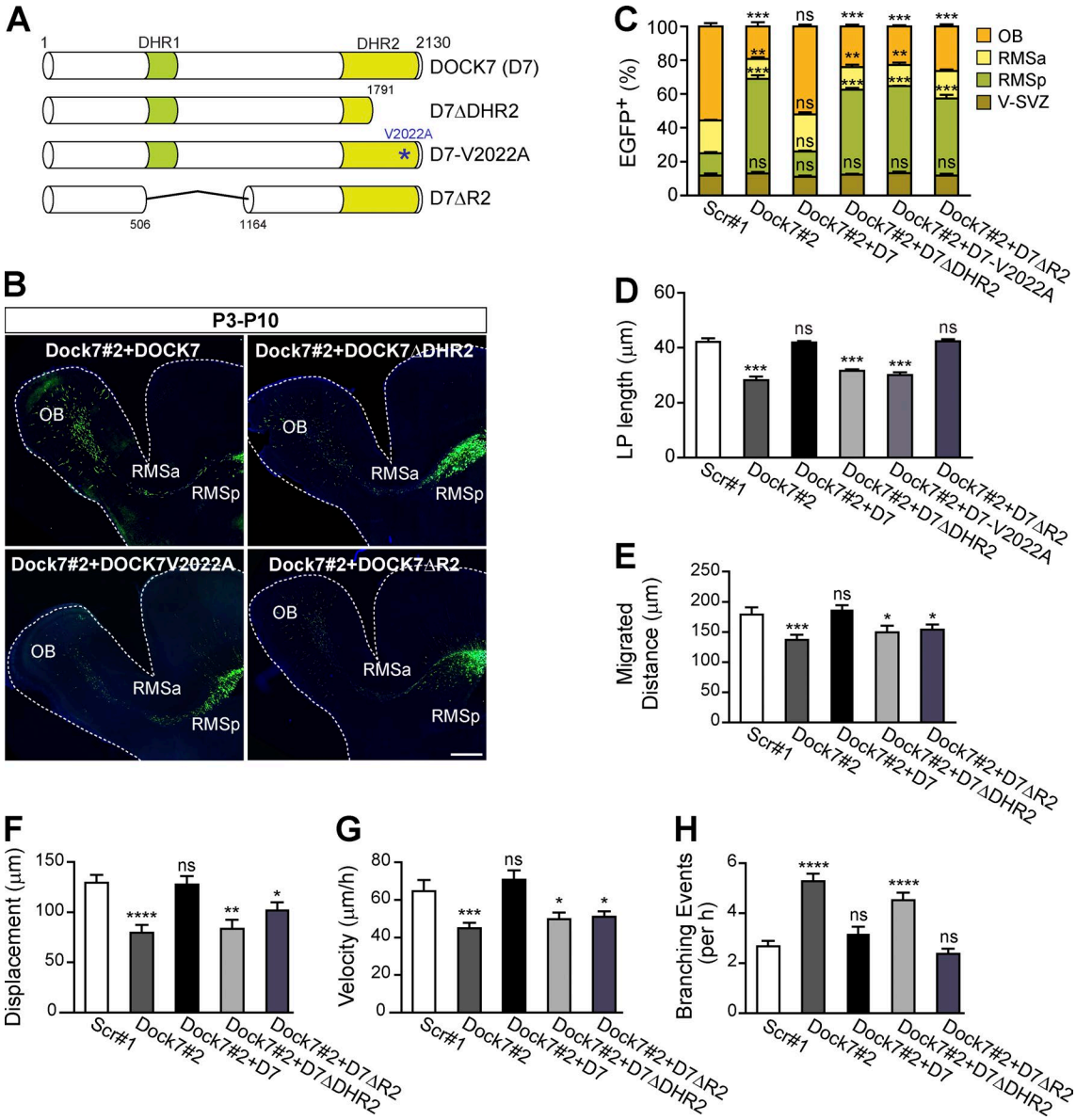

Figure 4. **DOCK7 controls different cellular aspects of neuroblast migration via DHR2/Rac-dependent and R2-dependent pathways.** (A) DOCK7 domain structure and deletion and point mutant constructs. ΔR2 comprises the DHR1 domain (amino acids 561–727) and TACC3-binding domain (amino acids 933–1,164). The asterisk indicates the DOCK7(V2022A) mutation. (B) Composite confocal images of forebrains of mice electroporated at P3 with plasmids expressing EGFP and Dock7#2 shRNA+DOCK7, Dock7#2 shRNA+DOCK7ΔDHR2, Dock7#2 shRNA+DOCK7V2022A, or Dock7#2 shRNA+DOCK7ΔR2 and sacrificed at P10, showing distribution of EGFP+ transfected neuroblasts along the V-SVZ–RMS–OB pathway. Slices were counterstained with DAPI. Dotted lines outline borders of sagittal slices. Bar, 500 µm. (C) Quantification of the distribution of EGFP+ transfected cells along the V-SVZ–RMS–OB pathway. *n* = 1,316–1,870 cells from at least three animals for each condition. (D) Quantification of the length of the LP of neuroblasts expressing indicated constructs. *n* = 91–680 cells from at least three animals for each condition. (E–H) P2–3 mouse pups were electroporated with a tdTomato-expressing plasmid together with one of the indicated constructs. Acute sagittal brain slices were prepared 5 d later and subjected to confocal live-cell imaging. Quantifications of the mean migrated distance (E), displacement (F), velocity (G), and number of branching events per h (H) for the tdTomato+ transfected neuroblasts. *n* = 42–61 cells from four to seven animals for each condition. Data are shown as means ± SEM. *, P < 0.05; **, P < 0.01; ***, P < 0.001; ****, P < 0.0001; ns, P > 0.05 compared with scr#1; one-way ANOVA with Dunnett's post hoc test.

was analyzed as described in the Dock7 depletion impairs the migration. . . section. We found that all three p116^{Rip} shRNAs impaired the migration of V-SVZ neuroblasts. Although most of the transfected cells in the control group were present in the RMSa and OB, many of the transfected cells in the p116^{Rip} shRNA groups were still located in the RMSp (Fig. 6, A and B; and Fig. S3, D and E). Notably, rescue experiments in which p116^{Rip}#1 shRNA was coexpressed with RNAi-resistant p116^{Rip} cDNA (Fig. S3, B and C) confirmed that the effect of p116^{Rip} RNAi on migration was specific (Fig. 6, A and B). Live-cell imaging studies further showed that p116^{Rip} shRNA-expressing cells migrated more slowly and that the migration distance and displacement were considerably reduced compared with control shRNA-expressing cells (Fig. 6, D–F; and Video 6). Importantly, as seen for cells coexpressing Dock7#2 shRNA and DOCK7ΔR2, the length of the LP of p116^{Rip} shRNA-expressing cells was not different from that of the control cells (Figs. 6 C and S3 F). Also, knockdown of p116^{Rip} did not affect the

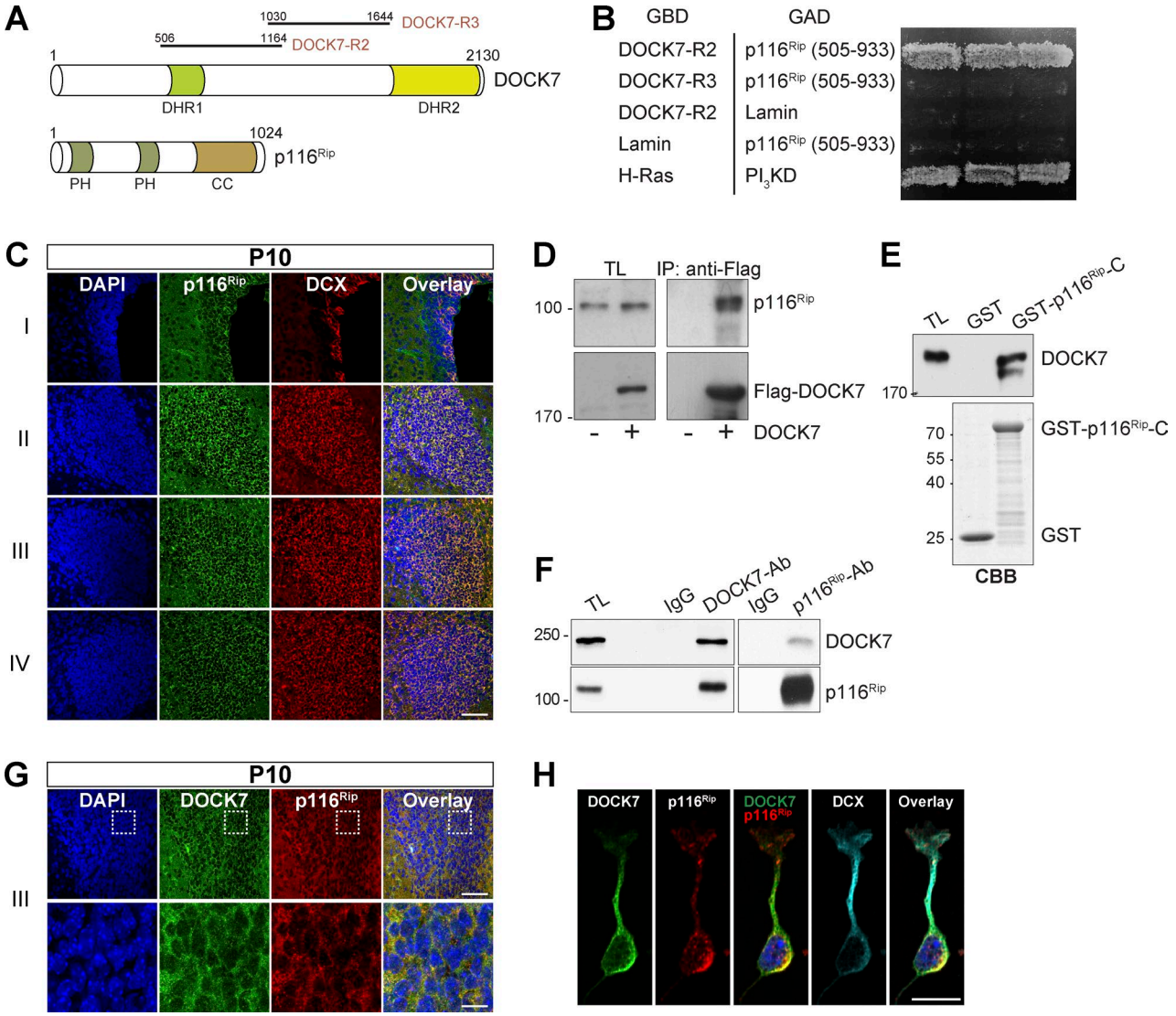

Figure 5. **DOCK7 interacts with p116Rip.** (A) DOCK7 and p116Rip domain structure. (Top) DOCK7 fragments used in YTH screen/testing. CC, coiled-coil domain; PH, pleckstrin homology domain. (B) YTH interaction between DOCK7-R2 and p116Rip. Yeast transformed with plasmids expressing DOCK7-R2 or DOCK7-R3 fused to GAL4 DNA–binding domain (GBD) and p116Rip-C (amino acids 505–933) fused to the GAL4-activation domain (GAD) were grown on medium lacking histidine. Lamin served as negative and H-Ras and phosphatidylinositol 3-OH–kinase-δ (PI_3KD) as positive controls. (C) Expression of p116Rip in DCX-positive neuroblasts along the V-SVZ–RMS–OB pathway. Coronal sections of P10 mouse forebrain at positions indicated in the cartoon in Fig. 1 A immunostained with antibodies to p116Rip and DCX and counterstained with DAPI. (D) DOCK7–p116Rip interaction in mammalian cells. Lysates from HEK293 cells transiently expressing Flag-DOCK7 or empty control vector were immunoprecipitated (IP) with an antibody to Flag and analyzed by immunoblotting with antibodies to Flag and p116Rip. TL, total lysate. (E) GST-p116Rip-C (amino acids 505–1,024) fusion protein or GST alone (bottom, Coomassie brilliant blue [CBB] staining), immobilized on beads, was incubated with lysates from P5 mouse brains. Bound DOCK7 was detected by immunoblotting with an antibody to DOCK7. (F) Interaction of DOCK7 and p116Rip in the brain. P10 mouse whole-brain extracts were immunoprecipitated with normal rabbit IgG, an anti-DOCK7 (DOCK7-Ab), or an anti-p116Rip (p116Rip-Ab) antibody and then were analyzed by immunoblotting with antibodies to DOCK7 and p116Rip. Molecular masses are shown in kilodaltons. (G and H) Colocalization of DOCK7 and p116Rip in V-SVZ–derived neuroblasts. (G) Coronal sections of P10 mouse forebrain at position III in the RMS as indicated in the cartoon in Fig. 1 A immunostained with antibodies to DOCK7 and p116Rip and counterstained with DAPI. Boxed regions are enlarged and shown at the bottom. (H) Neuroblasts dissociated from V-SVZ tissue of P1–3 mice were fixed at 30 h in vitro, followed by immunostaining with indicated antibodies and counterstained with DAPI. Bars: (C and G, top) 50 µm; (G, bottom, and H) 10 µm.

branching frequency of the neuroblasts' LP (Figs. 6 G and S3 H). Combined, these data are consistent with a role for p116Rip in mediating the R2-dependent function of DOCK7. Of note, p116Rip knockdown did not affect stem/progenitor cell proliferation nor neuroblast generation (Fig. S3 G and not depicted).

To substantiate that DOCK7's interaction with p116Rip is important for its function in migrating V-SVZ neuroblasts, we first examined whether ectopic expression of the R2 fragment of DOCK7 in neuroblasts interferes with their migration along the RMS. We found that this was indeed the case. The migration of neuroblasts ectopically expressing the R2 fragment was significantly impaired as compared with control neuroblasts (Fig. S4, A–C). Next, we further delineated the p116Rip-binding domain in DOCK7. To this end, DOCK7 mutants containing deletions in the R2 fragment were tested for their ability to bind to p116Rip in coimmunoprecipitation assays. Interestingly, we found that DOCK7Δ812–931 (henceforth referred to as DOCK7Δp116Rip) but not DOCK7ΔDHR1 (DOCK7Δ513–812) was impaired

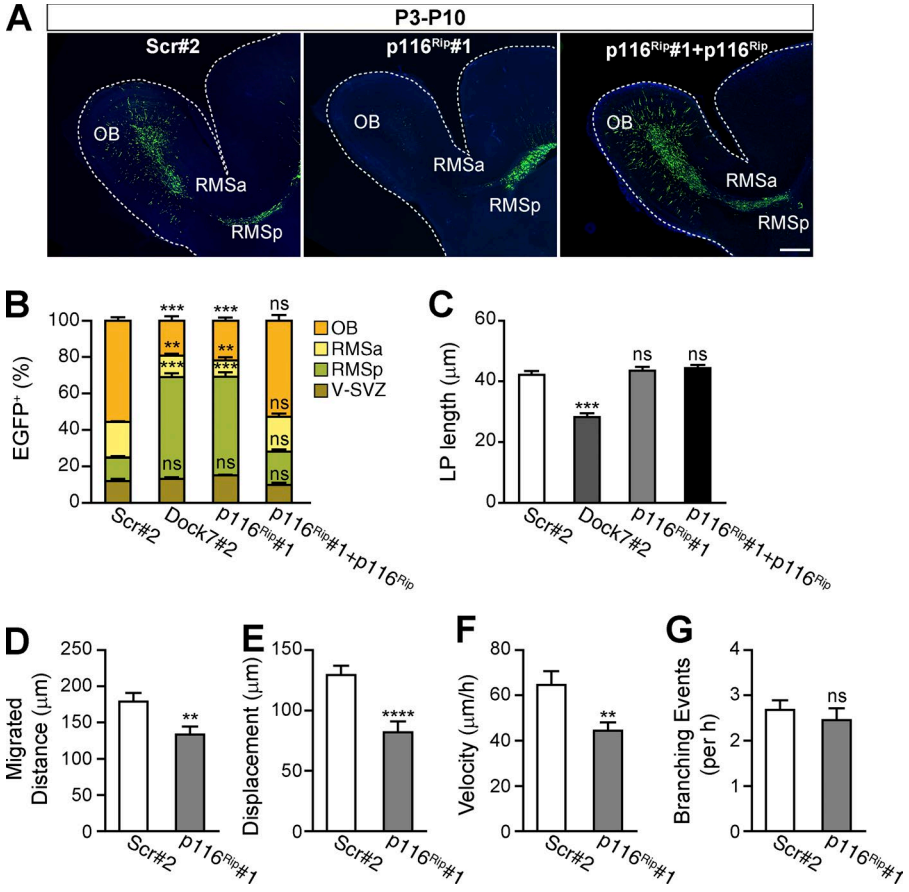

Figure 6. **Knockdown of p116^{Rip} impairs neuroblast migration along the RMS.** (A) Composite confocal images of forebrains of mice electroporated at P3 with plasmids expressing EGFP and scr#2 shRNA, p116^{Rip}#1 shRNA, or p116^{Rip}#1 shRNA together with RNAi-resistant p116^{Rip} and sacrificed at P10, showing distribution of EGFP$^+$ transfected neuroblasts along the V-SVZ–RMS–OB pathway. Slices were counterstained with DAPI. Dotted lines outline borders of sagittal slices. Bar, 500 µm. (B) Quantification of the distribution of EGFP$^+$ transfected cells along the V-SVZ–RMS–OB pathway. *n* = 816–2,100 cells from at least three animals for each condition. (C) Quantification of the length of the LP of neuroblasts expressing indicated constructs. *n* = 60–147 cells from at least three animals for each condition. (D–G) P2–3 mouse pups were electroporated with a tdTomato-expressing plasmid together with one of the indicated constructs. Acute sagittal brain slices were prepared 5 d later and subjected to confocal live-cell imaging. Quantification of the mean migrated distance (D), displacement (E), velocity (F), and number of branching events per h (G) for the tdTomato$^+$ transfected neuroblasts. *n* = 40–52 cells from five to six animals for each condition. Data are shown as means ± SEM. **, P < 0.01; ***, P < 0.001; ****, P < 0.0001; ns, P > 0.05 (B and C, compared with scr#2); one-way ANOVA with Dunnett's post hoc test (B and C) or Student's *t* test (D–G).

in p116^{Rip} binding (Fig. S4, A and D). We then examined the ability of the DOCK7Δp116^{Rip} mutant to rescue the DOCK7 RNAi-induced defects in neuroblast migration. Coexpression of DOCK7Δp116^{Rip} with Dock7#2 shRNA failed to rescue the DOCK7 RNAi-induced migration defect (Fig. 7, A and B) even though it did restore the defect in LP length (Fig. 7 C). Live-cell imaging studies further showed that the branching frequency of neuroblasts coexpressing Dock7#2 shRNA and DOCK7Δp116^{Rip} was not different from that of the control groups (Figs. 7 G and S4 E). In contrast, the motility of the cell body of these cells was considerably slowed compared with that of control neuroblasts (Fig. 7 F, Fig. S4 E, and Video 7), and in accordance, the migration distance and displacement of these cells were significantly reduced (Fig. 7, D and E). Thus, in neuroblasts deficient in DOCK7/p116^{Rip} signaling, there is a defect in the forward migration of the cell body, but not in LP formation/extension, suggesting that the p116^{Rip} interaction with DOCK7 controls nucleokinesis in tangentially migrating V-SVZ neuroblasts.

DOCK7 via p116^{Rip} controls somal translocation through F-actin remodeling at the cell rear

Nucleokinesis is a two-step process, with centrosome movement preceding that of the nucleus and cell soma (Schaar and McConnell, 2005; Tsai and Gleeson, 2005; Métin et al., 2008; Trivedi and Solecki, 2011). Hence, to further establish the role of the DOCK7–p116^{Rip} complex in regulating nucleokinesis and to gain insight into how it does so, we set out to monitor the centrosome and cell soma dynamics during nucleokinesis in neuroblasts deficient in DOCK7/p116^{Rip} signaling. To accomplish this, we resorted to an in vitro model system for V-SVZ neuroblast migration in which neuroblasts isolated from V-SVZ tissue are cultured in a 3D Matrigel matrix (Falenta et al., 2013). The advantage of this system is that it allows for higher-resolution imaging. Before starting time-lapse imaging, we first verified that this model system recapitulated the migration phenotypes we observed in brain slices. Neuroblasts isolated from postnatal V-SVZ tissue were cotransfected with an EGFP-expressing plasmid and one of the indicated constructs (Fig. S5). The cells were then reaggregated, embedded in Matrigel, and left to migrate for 30 h before immunostaining for GFP and βIII-tubulin. In concurrence with our findings in brain slices, neuroblasts expressing p116^{Rip}#1 shRNA or Dock7#2 shRNA together with DOCK7Δp116^{Rip} displayed impaired Matrigel migration while exhibiting a polarized morphology with an intact LP (Fig. S5, A–C). Indeed, the migration distance for these cells was reduced by >40% compared with the control neuroblasts (Fig. S5 C).

We then performed time-lapse imaging and tracked the movements of the centrosome and cell soma during the migration of transfected neuroblasts in Matrigel. The centrosome was visualized with the pericentrin-AKAP450 centrosomal targeting domain fused to monomeric Kusabira Orange (PACT-mKO1; Sakakibara et al., 2014), which was coexpressed with EGFP and one of the indicated constructs. As expected, in control neuroblasts expressing either scr#2 shRNA or Dock7#2 shRNA together with DOCK7, we observed that the centrosome migrated away from the nucleus into the proximal region of the LP before somal translocation. Then, after a peak in the

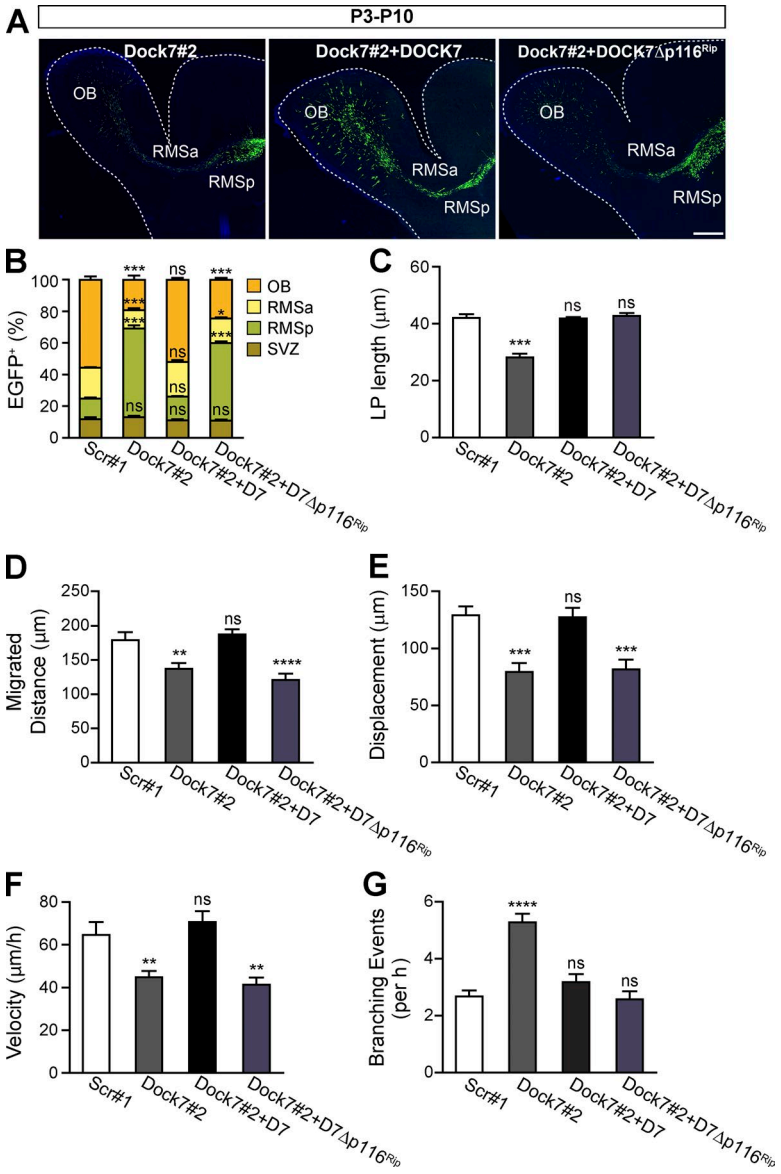

Figure 7. **DOCK7 interaction with p116Rip is essential for neuroblast migration along the RMS.** (A) Composite confocal images of forebrains of mice electroporated at P3 with plasmids expressing EGFP and Dock7#2, Dock7#2 + DOCK7, or Dock7#2 + DOCK7Δp116Rip and sacrificed at P10, showing distribution of EGFP+ transfected neuroblasts along the V-SVZ–RMS–OB pathway. Slices were counterstained with DAPI. Dotted lines outline borders of sagittal slices. Bar, 500 µm. (B) Quantification of the distribution of EGFP+ transfected cells along the V-SVZ–RMS–OB pathway. *n* = 1,316–1,791 cells from at least three animals for each condition. (C) Quantification of the length of the LP of neuroblasts expressing indicated constructs. *n* = 91–680 cells from at least three animals for each condition. (D–G) P2–3 mouse pups were electroporated with a tdTomato-expressing plasmid together with one of the indicated constructs. Acute sagittal brain slices were prepared 5 d later and subjected to confocal live-cell imaging. Graphs show quantifications of the mean migrated distance (D), displacement (E), velocity (F), and number of branching events per h (G) for the tdTomato+ transfected neuroblasts. *n* = 50–61 cells from five to seven animals for each condition. Data are shown as means ± SEM. *, P < 0.05; **, P < 0.01; ***, P < 0.001; ****, P < 0.0001; ns, P > 0.05 compared with scr#1; one-way ANOVA with Dunnett's post hoc test.

N–C distance (distance between the leading edge of nucleus and centrosome), the cell body swiftly translocated toward the centrosome (Fig. 8, A–F; and Videos 8 and 10). Interestingly, although in neuroblasts deficient in DOCK7/p116Rip signaling (p116Rip#1 shRNA– or Dock7#2 shRNA+DOCK7Δp116Rip–expressing cells), the centrosome was observed to initially move forward into the proximal LP, reaching a maximum N–C distance similar to that of the control neuroblasts, the cell body did not translocate at the proper rate (Fig. 8, A–F; and Videos 9 and 11). Compared with the control neuroblasts, the mean velocity of the cell body movements and the number of somal translocation events (defined as cell body movements over a distance of 1 µm per 1 min) were greatly reduced in neuroblasts expressing p116Rip#1 shRNA or Dock7#2 shRNA together with DOCK7Δp116Rip (Fig. 8, D and E). Consequently, in these cells, the movement of the centrosome became unstable, and we often observed the centrosome falling back toward the nucleus after an N–C peak rather than the nucleus translocating toward the centrosome (Videos 9 and 11). These results indicate that DOCK7/p116Rip-mediated signaling is critical for somal translocation but not centrosomal forward movement. Noteworthy, in neuroblasts expressing Dock7#2 shRNA by itself, somal translocation was impeded, similarly as seen in cells expressing Dock7#2 shRNA together with DOCK7Δp116Rip (Fig. 8, A, C, D, and E; and Video 12). In addition, we observed that the forward movement of the centrosome was impeded as well (Fig. 8, A, B, and F; and Video 12). This finding was expected because DOCK7 not only affects a p116Rip- but also a Rac-dependent pathway. Centrosome positioning, like LP extension, is dependent on MT growth/stability, the latter we previously showed to be regulated by DOCK7 via Rac activation (Watabe-Uchida et al., 2006).

Previous studies have reported that somal translocation in tangentially migrating interneurons including V-SVZ neuroblasts requires actin remodeling and condensation at the rear of the cell and that actomyosin contraction at this site plays a prominent role in pushing the cell body forward (Bellion et al., 2005; Schaar and McConnell, 2005; Martini and Valdeolmillos, 2010; Godin et al., 2012; Shinohara et al., 2012; Tielens et al., 2016). Given that p116Rip has been shown to bind F-actin and to modulate the actomyosin-based cytoskeleton (Mulder et al., 2003, 2004; Riddick et al., 2008), we therefore examined

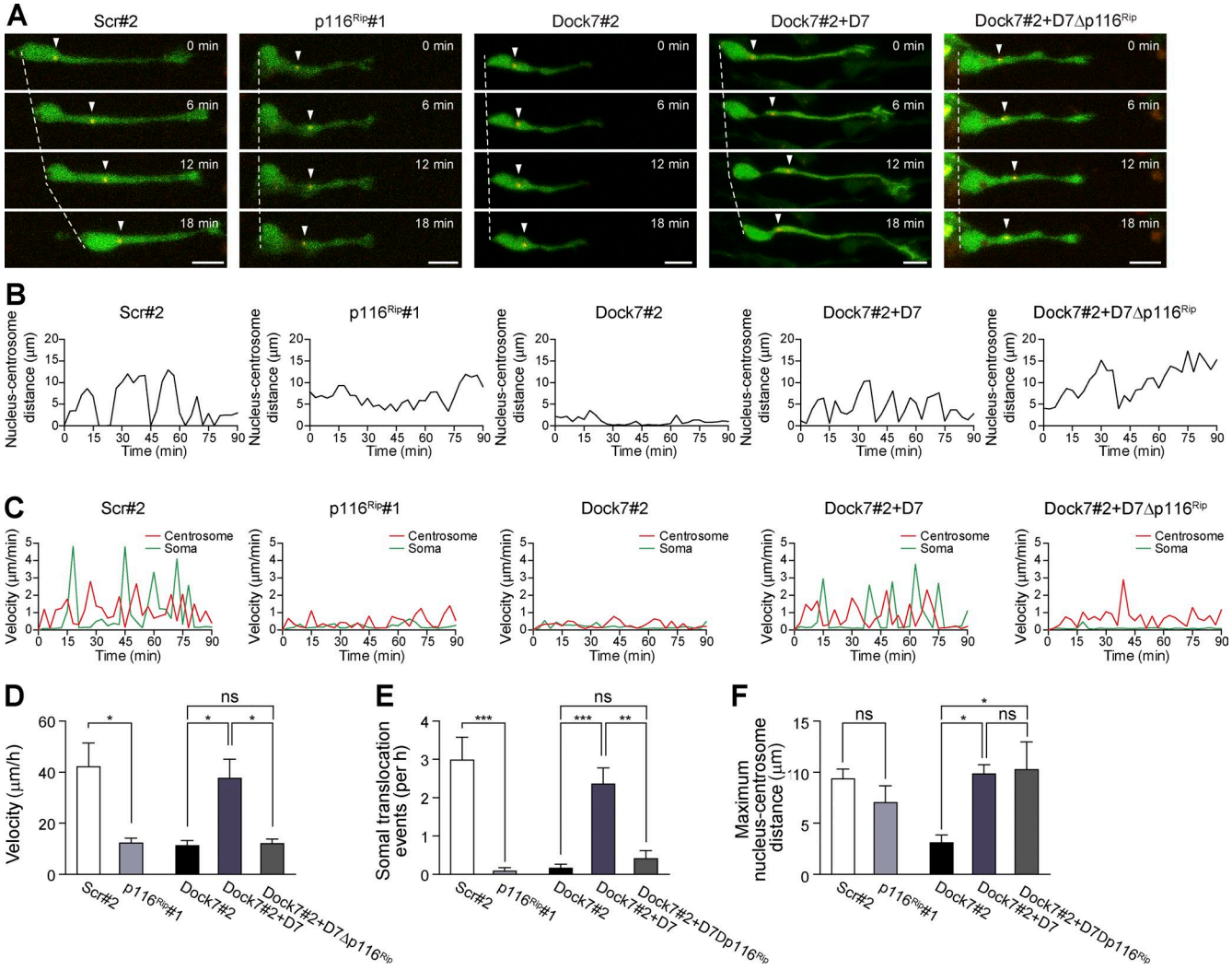

Figure 8. **DOCK7/p116Rip signaling controls somal translocation.** (A–F) Neuroblasts dissociated from the V-SVZ of P1–3 mice were coelectroporated with one of the indicated constructs and a plasmid coexpressing EGFP and PACT-mKO1, a marker for the centrosome. Cells were reaggregated, embedded in Matrigel, and subjected to confocal live-cell imaging. (A) Examples of time-lapse series showing centrosome and cell soma movements during migration in neuroblasts transfected with indicated constructs. Images are taken from Videos 8–12. Signals of EGFP and PACT-mKO1 are shown in green and red, respectively. White dashed lines indicate advancement of the rear edge of each cell. Arrowheads indicate centrosome position. Bars, 10 µm. (B and C) Temporal changes in the distance between the nucleus and the centrosome (N–C distance; B) and velocity of the cell body (green lines) and the centrosome (red lines; C) in migrating neuroblasts expressing indicated constructs. (D–F) Quantification of velocity (D), somal translocation events (E), and maximum nucleus–centrosome distance (F) for neuroblasts expressing indicated constructs. *n* = 6 cells (scr#2); *n* = 5 cells (p116Rip#1); *n* = 7 cells (Dock7#2); *n* = 12 cells (Dock7#2 + DOCK7); and *n* = 8 cells (Dock7#2 + DOCK7Δp116Rip); from 5–12 animals for each condition. Data are shown as means ± SEM. *, P < 0.05; **, P < 0.01; ***, P < 0.001; ns, P > 0.05; one-way ANOVA with Dunnett's post hoc test.

the dynamics of F-actin to see whether they are changed in neuroblasts deficient in DOCK7/p116Rip signaling by using Lifeact-EGFP. Consistent with previous studies (Martini and Valdeolmillos, 2010; Shinohara et al., 2012), we observed that in control neuroblasts, F-actin began to condense at the cell rear immediately before the onset of somal movement. This condensation then grew to form a cup-shaped F-actin structure and ended up in a spot at the base of the trailing process at the end of the active phase of somal movement (Fig. 9 A). Strikingly, in neuroblasts expressing p116Rip#1 shRNA or Dock7#2 shRNA together with DOCK7Δp116Rip, no evident F-actin condensation or formation of a cup-shaped F-actin structure at the cell rear was observed (Fig. 9 A). In contrast, F-actin signals in the proximal domain and at the tip of the LP appeared undisturbed in these neuroblasts. Collectively, these data support a model in which DOCK7/p116Rip-mediated signaling regulates F-actin remodeling and condensation at the cell rear to drive somal translocation in migrating V-SVZ neuroblasts. In support of this model, we observed that both DOCK7 and p116Rip accumulated at the cell rear of WT V-SVZ neuroblasts captured just before and during somal translocation (Fig. 9 B).

Discussion

The migration of V-SVZ neuroblasts along the RMS in the postnatal forebrain is a critical process necessary for the continuous remodeling of OB neural circuits throughout life (Arenkiel, 2010; Belvindrah et al., 2011; Lazarini and Lledo, 2011; Sawada and Sawamoto, 2013; Obernier et al., 2014; Sakamoto et al., 2014; Sailor et al., 2017). Although substantial progress has been made toward identifying extracellular factors and matrix

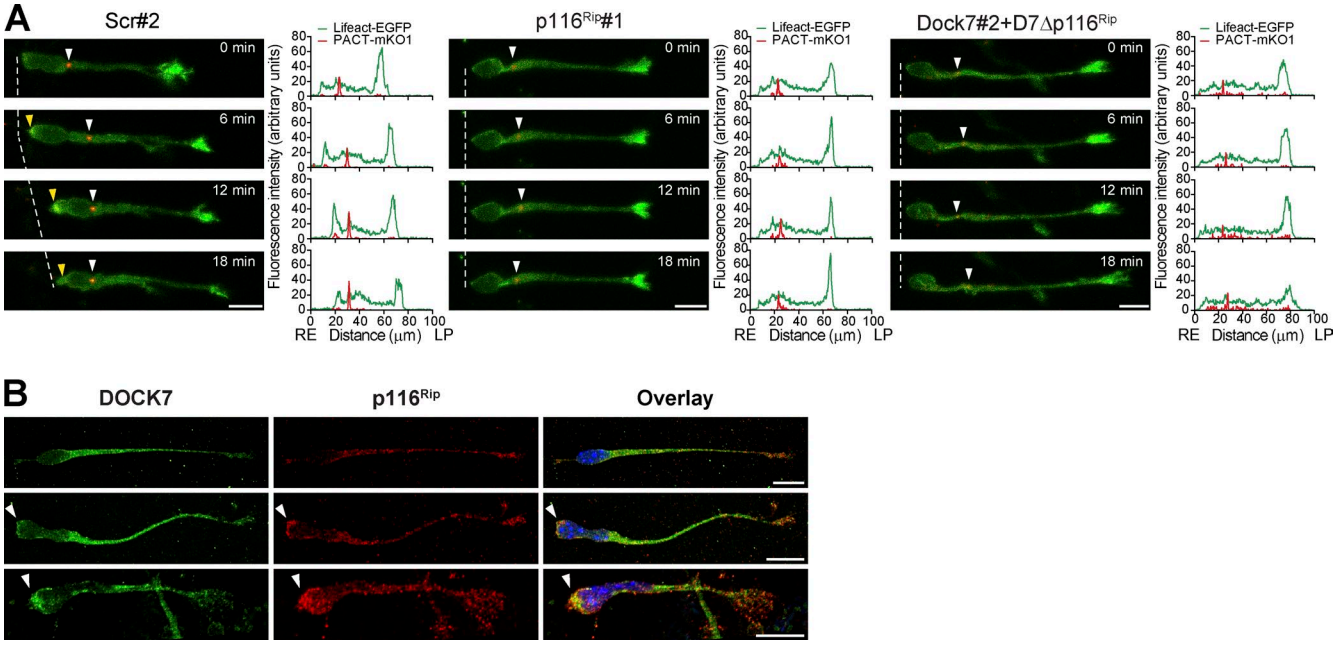

Figure 9. **DOCK7/p116Rip signaling controls somal translocation through F-actin remodeling at the cell rear.** (A) Neuroblasts dissociated from the V-SVZ of P1–3 mice were coelectroporated with one of the indicated constructs and a plasmid coexpressing Lifeact-EGFP, a marker for F-actin, and PACT-mKO1. Cells were reaggregated, embedded in Matrigel, and subjected to confocal live-cell imaging. Examples of time-lapse series showing F-actin remodeling during migration in neuroblasts transfected with indicated constructs. Signals of Lifeact-EGFP and PACT-mKO1 are shown in green and red, respectively. White dashed lines indicate advancement of the rear edge (RE) of each cell. White and yellow arrowheads indicate position of centrosome ahead of the nucleus and formation of F-actin condensation at the cell rear, respectively. Linescan profiles to the left of each image show the signal intensities of Lifeact-EGFP (green lines) and PACT-mKO1 (red lines) from the rear edge of the cell soma to the tip of the LP in the corresponding images. Representative images of a total of 5–12 independent experiments/condition are shown. (B) Enrichment of DOCK7 and p116Rip signals at the cell rear during somal translocation. Reaggregated neuroblasts isolated from V-SVZ tissue of P1–3 mice were embedded in Matrigel and allowed to migrate for 30 h before immunostaining for DOCK7 and p116Rip. Representative images of neuroblasts captured before (top two rows) and during somal translocation (bottom row) are shown. Enrichment of DOCK7 and p116Rip signals at the cell rear just before and during somal translocation is indicated by arrowheads. Bars, 10 µm.

components that guide the migration of these cells to the OB (Ghashghaei et al., 2007; Leong and Turnley, 2011; Lalli, 2014; Lim and Alvarez-Buylla, 2016), remarkably little is known about the intrinsic factors that govern the dynamic reshaping of the neuroblasts' morphology required to ensure their proper migration along the RMS. In this study, we present evidence that DOCK7, a member of the DOCK180 family of atypical RhoGEFs, regulates tangential migration of V-SVZ neuroblasts by controlling both LP extension and nucleokinesis and that it does so by acting on distinct pathways. Namely, DOCK7 controls LP stability/growth via a DHR2/Rac-dependent pathway, likely by modulating MT networks while also regulating F-actin remodeling at the cell rear to promote somal/nuclear translocation via a previously unrecognized p116Rip-dependent pathway. The coordinated action of both pathways is required to ensure efficient migration of V-SVZ neuroblasts along the RMS.

After birth in the postnatal/adult V-SVZ, stem cell–derived neuroblasts undertake a remarkable journey, migrating a distance of ∼3–8 mm along the RMS en route to the OB (Luskin, 1993; Lois and Alvarez-Buylla, 1994; Ghashghaei et al., 2007; Lim and Alvarez-Buylla, 2016). Our data show that DOCK7 is present along the V-SVZ–RMS–OB pathway of the postnatal mouse forebrain, where it is prominently expressed in migratory neuroblasts, and most importantly, they unveil a critical role for DOCK7 in the tangential migration of these cells. Indeed, silencing of DOCK7 resulted in impaired/delayed neuroblast migration, with many of the DOCK7-depleted cells still residing in the posterior part of the RMS >1 wk after their generation in the V-SVZ. The cells at this location displayed increased branching frequency, a more exploratory behavior, and reduced migration velocity, indicating that DOCK7 function is critical for the morphological changes required for proper V-SVZ neuroblast migration (see below). Notably, our data also imply that other DOCK180 family members (Miyamoto and Yamauchi, 2010; Gadea and Blangy, 2014; Laurin and Côté, 2014) do not compensate for this function of DOCK7, as knockdown of DOCK7 alone was sufficient to cause the defect in V-SVZ neuroblast migration.

Our work further explored the mechanisms by which DOCK7 controls the migration of V-SVZ–derived neuroblasts in the postnatal RMS. Our live-cell imaging experiments showed that neuroblasts depleted of DOCK7 displayed shorter and more highly branched LPs and a marked reduction in the forward movement of the cell body. Although these data revealed the requirement for DOCK7 in the stabilization and growth of the LP, they failed, however, to unveil whether DOCK7 is directly involved in somal translocation, as the defect in cell body movement could be secondary to LP abnormalities. By using a molecular replacement strategy in which expression of endogenous DOCK7 was reduced via RNAi and replaced by distinct mutant forms of DOCK7, we were able to uncover that DOCK7 governs the migration of neuroblasts by regulating both LP stability/growth and somal translocation via DHR2/Rac-dependent and R2-dependent pathways, respectively. Indeed, although replacement of endogenous DOCK7 with either DOCK7ΔDHR2 or DOCK7ΔR2 mutants, with the former but not the latter being defective in Rac activation, resulted in migration defects, and only neuroblasts expressing DOCK7ΔDHR2

displayed LP abnormalities. Notably, the requirement of the catalytic DHR2 domain in mediating LP stability/growth is in line with our previous research implicating a DOCK7 DHR2/Rac-dependent pathway in the regulation of axon elongation in developing neurons (Watabe-Uchida et al., 2006). More specifically, we showed that this promotion of axon elongation is dependent on DOCK7's ability to enhance MT growth through Rac activation. Thus, as MT growth and stability are required for LP extension and function (Koizumi et al., 2006), we envision that DOCK7 could similarly increase MT growth in the dominant process of V-SVZ neuroblasts to promote LP extension. In accordance, we observed prominent staining and strong colocalization of DOCK7 with MTs in the shaft of the LP and the proximal region of the growth cone–like structure.

Rather unanticipated were our findings pointing to the requirement of a DOCK7 R2-dependent pathway in the forward migration of the cell soma but not LP extension, which prompted us to further investigate the underlying mechanism or mechanisms. In a search for binding partners of the R2 fragment of DOCK7, we identified the myosin phosphatase–RhoA–interacting protein p116^{Rip}, an F-actin binding protein previously implicated in the regulation of the actomyosin-based cytoskeleton in nonneuronal cultured cells (Mulder et al., 2003, 2004; Riddick et al., 2008). The role, though, of p116^{Rip} in the migration of neuronal precursors or in fact of any cell type had not been investigated. We found that p116^{Rip} is expressed in migratory V-SVZ neuroblasts of the postnatal forebrain. In these cells, it displays significant overlapping staining with DOCK7, which was particularly noticeable at the cell rear during somal translocation, a site where F-actin also accumulates transiently (Shinohara et al., 2012). Most importantly, we found that silencing of p116^{Rip} impaired the migration of V-SVZ neuroblasts and that this impairment resulted from a defect in the forward translocation of the cell soma/nucleus but not LP extension. Similar migration phenotypes were observed in neuroblasts in which endogenous DOCK7 was replaced by DOCK7 mutants defective in p116^{Rip} binding. Collectively, these results unveiled a key role for p116^{Rip} in mediating the R2-dependent function of DOCK7 in somal translocation of migrating V-SVZ neuroblasts.

Although the mechanisms underlying somal translocation in tangentially migrating interneuron precursors remain incompletely understood, several studies have reported that actin remodeling and condensation coordinated by actomyosin contractility at the cell rear play a prominent role in driving the cell soma/nucleus forward (Bellion et al., 2005; Schaar and McConnell, 2005; Martini and Valdeolmillos, 2010; Godin et al., 2012; Shinohara et al., 2012). During the migration cycle of V-SVZ neuroblasts, F-actin condenses at the rear of the cell, forming a cup-shaped F-actin structure (Shinohara et al., 2012). Consistent with these studies, our real-time imaging of Lifeact-EGFP revealed F-actin condensation and the formation of a transient cup-shaped F-actin structure at the cell rear during somal translocation in control V-SVZ neuroblasts. In contrast, knockdown of p116^{Rip} or disruption of the DOCK7/p116^{Rip} interaction abolished the formation of the cup-shaped F-actin structure at the cell rear. Previous studies have shown that the formation of this F-actin structure and actomyosin-based contractility in migrating V-SVZ neuroblasts are mediated by the Rho effectors mDia and ROCK (Leong et al., 2011; Shinohara et al., 2012). Specifically, mDia generates actin filaments, whereas ROCK facilitates the activation of MLC by activating MLCK or inactivating MLCP to promote actomyosin contractility, and together they help drive the forward translocation of the cell soma/nucleus. As p116^{Rip} has been shown to interact with both RhoA and MLCP (Gebbink et al., 1997; Surks et al., 2003), the interaction of DOCK7 with p116^{Rip} likely regulates F-actin remodeling and actomyosin contractility through regulation of RhoA signaling pathways. It is important to note, however, that the precise function of p116^{Rip} remains unclear and appears to some extent cell type dependent (Gebbink et al., 1997; Mulder et al., 2003, 2004; Koga and Ikebe, 2005; Riddick et al., 2008). An increasing number of studies suggest that p116^{Rip} does not affect the activities of RhoA/ROCK but rather acts as a scaffold linking the RhoA/ROCK pathway and the MLCP complex to the F-actin cytoskeleton to thereby modulate actomyosin contractility (Mulder et al., 2004; Surks et al., 2005; Riddick et al., 2008). These data, combined with our findings that DOCK7 and p116^{Rip} are localized to the cell rear during nucleokinesis and that both proteins are critical for the translocation of the cell soma/nucleus, suggest that DOCK7/p116^{Rip} signaling localizes key RhoA signaling components at the cell rear to regulate actin cytoskeletal remodeling and actomyosin dynamics required for somal translocation in tangentially migrating V-SVZ–derived neuroblasts.

It should be noted that in addition to the F-actin accumulation/condensation at the cell rear required for somal translocation, F-actin accumulation (albeit less intense) in the proximal LP preceding somal/nuclear movement has been observed in migrating V-SVZ neuroblasts, and it has been suggested that mDia-dependent anterograde F-actin movement plays a role in centrosome positioning (Shinohara et al., 2012). In contrast with mDia depletion, we did not observe any major effect on F-actin staining or movement in the proximal LP upon knockdown of p116^{Rip} or disruption of the DOCK7–p116^{Rip} complex. This is in line with our live imaging studies showing that DOCK7/p116^{Rip}-mediated signaling is not essential for the positioning of the centrosome per se but rather for the translocation of the cell soma/nucleus toward the centrosome (Fig. 8). Our data do show, however, that DOCK7 is required for centrosome positioning independent of p116^{Rip} signaling. We envision that DOCK7 controls this process by promoting MT growth/stability via a Rac-dependent pathway, similarly as for LP extension.

In summary, our study provides novel mechanistic insight into the molecular basis of LP extension and somal/nuclear translocation during V-SVZ neuroblast migration in the RMS of the postnatal forebrain. It reveals that DOCK7 serves two important functions that support neuroblast migration: it controls LP stability/growth via a DHR2/Rac-dependent pathway, likely by controlling MT stabilization/growth in the LP, and it promotes somal translocation through F-actin remodeling at the cell rear via a p116^{Rip}-dependent pathway. Both functions contribute to the dynamic remodeling of neuroblast morphology required to ensure proper tangential migration. In the future, it will be interesting to determine the intricacies of the DOCK7/Rac and DOCK7/p116^{Rip}-mediated interactions and to identify the extrinsic signals that regulate the spatiotemporal localization of DOCK7 and its interacting proteins and signaling pathways in migrating V-SVZ–derived neuroblasts.

Materials and methods

DNA constructs

pCAGGS-AFP (EGFP), pCAGGS-tdTomato, pCAGGS-Flag-DOCK7, and pCAGGS-Flag-DOCK7ΔDHR2 constructs have been described

previously (Watabe-Uchida et al., 2006; Yang et al., 2012). cDNAs encoding DOCK7Δ506–1,164 (DOCK7ΔR2), DOCK7Δ513–812 (DOCK7ΔDHR1), DOCK7Δ812–931 (DOCK7Δp116^{Rip}), and DOCK7 506–1,164 (DOCK7-R2) were subcloned into pCAGGS with the addition of an N-terminal Flag epitope tag. The pCAGGS-Flag-DOCK7-V2022A mutant was generated using the QuikChange Site-Directed Mutagenesis kit (Agilent Technologies) according to the manufacturer's protocol and using the following oligonucleotide primers: 5′-GGTACTCCAGGGATCTGTAGGCACCACAGCGAA TCAGGGGCCTTTGGAAGTTGCCCAGG-3′ and 5′-CCTGGGCAA CTTCCAAAGGCCCCTGATTCGCTGTGGTGCCTACAGATCCCT GGAGTACC-3′. pcDNA-HA-p116^{Rip} and pcDNA-EGFP-p116^{Rip} plasmids were provided by W. Moolenaar (The Netherlands Cancer Institute, Amsterdam, Netherlands; Mulder et al., 2004). cDNAs encoding p116^{Rip}-WT and RNAi-resistant p116^{Rip} (see further below) were subcloned into pCAGGS with the addition of an N-terminal HA epitope tag. The GST-p116^{Rip}-C construct was obtained by subcloning a cDNA fragment encoding amino acids 505–1,024 of mouse p116^{Rip} into pGEX-4T2 (GE Healthcare). The YTH constructs pGBD-DOCK7-R2 and -R3 were generated by insertion of cDNAs encoding amino acids 506–1,164 (R2) and 1,030–1,644 (R3) of DOCK7 into pPC97 (Yang et al., 2012). pGAD-p116^{Rip} (amino acids 505–933) was obtained in YTH screen. pGBD-lamin, pGBD–H-Ras, pGAD-lamin, and pGAD-PI3KD were generated by subcloning cDNAs encoding lamin, H-Ras, and PI3-kinase δ into pPC86 and pPC97, respectively (Yang et al., 2012). pTα-LPL-PACT-mKO1 plasmid was provided by A. Sakakibara (Chubu University, Kasugai, Japan; Sakakibara et al., 2014). pCAGGS-EGFP-P2A-PACT-mKO1 was generated by subcloning the PACT-mKO1 cDNA fragment from pTα-LPL-PACT-mKO1 into pCAGGS-EGFP-P2A-MCS. pCMV-mEGFP–Lifeact-7 was provided by M. Davidson (Florida State University, Tallahassee, FL) through the Addgene plasmid repository (54610; Addgene). pCAGGS-mEGFP–Lifeact-7–P2A-PACT-mKO1 was generated by subcloning mEGFP–Lifeact-7 and P2A-PACT-mKO1 cDNA fragments from pCMV-mEGFP–Lifeact-7 and pCAGGS-EGFP-P2A-PACT-mKO1, respectively, into pCAGGS. For RNAi experiments, previously described DNA fragments encoding shRNAs directed against mouse DOCK7 mRNA (Dock7#1, 5′-GCT AATCGGGATGCAAAGA-3′; and Dock7#2, 5′-GGTACAGTACAC ATTTACA-3′; Watabe-Uchida et al., 2006; Yang et al., 2012) and those directed against mouse p116^{Rip} mRNA (p116^{Rip}#1, 5′-GAGCAAGTG TCAGAACTGC-3′; p116^{Rip}#2, 5′-GGTCCCAGGTAATTGAGAA-3′; and p116^{Rip}#3, 5′-GAGCACATGGAAACCAACA-3′; Mulder et al., 2004; Koga and Ikebe, 2005) were cloned into pSUPER (Oligoengine). To generate p116^{Rip} cDNA resistant to p116^{Rip}#1 shRNA, the sequence 5′-GAGCAAGTGTCAGAACTGC-3′ was changed to 5′-GAGtA-AaTGTCAaAACTGC-3′ (lowercase letters show changes). p116^{Rip} shRNA #1 resistant point mutants were generated on pCAGGS-HA-p116^{Rip} using the PrimeSTAR Mutagenesis Basal kit (Takara Bio Inc.) according to the manufacturer's protocol and using the following oligonucleotide primers: 5′-AGTAAATGTCAAAACTGCTTCAAGCCC CGC-3′ and 5′-GTTTTGACATTTACTCTTGTTGAAGATGTTG-3′.

YTH screening

5×10^5 clones of an adult mouse brain cDNA library in the pPC86 vector were screened using the DOCK7-R2 fragment cloned into pPC97 as bait in the PJ69a yeast reporter strain (Van Aelst, 1998).

Cell culture and transfection

HEK293, HEK293T, HeLa, and Neuro-2a cells were cultured in DMEM containing 10% FBS (HyClone), 4 mM L-glutamine (Thermo Fisher Scientific), 100 U/ml penicillin (Thermo Fisher Scientific), and 100 µg/ml streptomycin (Thermo Fisher Scientific). Primary dissociated cultures of cortical neurons were prepared from E15.5 embryos of WT CD1 mice as previously described (Watabe-Uchida et al., 2006). In brief, brains of E15.5 embryos were removed, the cerebral meninges stripped, and cerebral cortices collected. Cortical tissue was minced and then digested using 0.75 mg/ml trypsin ($1–2 \times 10^3$ U/mg) for 30 min at 37°C. Cells were suspended and maintained in neurobasal medium (Thermo Fisher Scientific) containing 2% B27 and 2 mM GlutaMAX (Thermo Fisher Scientific). For the preparation of dissociated cultures of V-SVZ neuroblasts, V-SVZ tissue was dissected from P1–3 CD1 mice and dissociated with papain solution (Sigma-Aldrich). After trituration, the cells were plated onto glass coverslips coated with poly-D-lysine (Sigma-Aldrich) and laminin (Invitrogen) and then cultured in neurobasal medium containing 2% B27 and 1 mM GlutaMAX. HEK293 and HEK293T cells were transfected using the calcium phosphate coprecipitation method or the polyethylenimine transfection protocol (Yu et al., 2015). Neuro-2a cells were transfected using Lipofectamine 2000 reagent (Thermo Fisher Scientific) according to the manufacturer's protocol. Dissociated V-SVZ neuroblasts and cortical neurons were transfected using the Amaxa nucleofection system (Lonza; Yang et al., 2012).

Coimmunoprecipitation, GST pulldown assay, and Western blot analysis

For coimmunoprecipitation experiments using HEK293 cells expressing WT or mutant versions of Flag-DOCK7, cells were homogenized in ice-cold lysis buffer containing 50 mM Tris, pH 7.4, 1% NP-40, 200 mM NaCl, 2.5 mM $MgCl_2$, 10% glycerol, and protease inhibitors (Roche). Total lysates were incubated with mouse monoclonal anti-Flag M2-agarose beads (A2220; Sigma-Aldrich) overnight at 4°C. Beads were washed six times with lysis buffer. Immunoprecipitates were then resolved by SDS-PAGE and immunoblotted with mouse monoclonal anti-p116^{Rip} (1:1,000; R79520; BD) and mouse monoclonal anti-Flag M2 (1:1,000; F3165; Sigma-Aldrich) antibodies. For coimmunoprecipitation experiments using mouse whole-brain extracts, P10 CD1 brains were homogenized in radioimmunoprecipitation assay (RIPA) buffer (50 mM Tris HCl, pH 7.4, 150 mM NaCl, 1 mM EDTA, 1% NP-40, 0.5% sodium deoxycholate, 0.1% SDS, and protease inhibitors) and centrifuged at 21,000 *g* for 10 min at 4°C. The supernatants were incubated with rabbit polyclonal anti-DOCK7 (ab118790; Abcam), rabbit polyclonal anti-p116^{Rip} (NBP1-81035; Novus Biologicals), or normal rabbit IgG (2729; Cell Signaling Technology) antibody for 1 h at 4°C followed by 1 h incubation with Protein G Mag Sepharose (GE Healthcare). Beads were washed four times with RIPA buffer, and immunoprecipitates were then resolved by SDS-PAGE and immunoblotted with rabbit polyclonal anti-p116^{Rip} (1:1,000; NBP1-81035; Novus Biologicals) and rabbit polyclonal anti-DOCK7 (1:500, Watabe-Uchida et al., 2006) antibodies. For GST pulldown assays, GST-p116^{Rip}-C fusion protein and GST alone were immobilized onto Glutathione Sepharose beads (GE Healthcare). Brains collected from P5 CD1 mice were homogenized using micropestles (Eppendorf) in lysis buffer (50 mM Tris, pH 7.5, 1% Triton X-100, 150 mM NaCl, 5% glycerol, 5 mM NaF, 1 mM Na_3VO_4, and protease inhibitors). Equal amounts of total lysates were incubated with GST-p116^{Rip}-C fusion protein or GST. Immunoblots were probed with rabbit polyclonal anti-DOCK7 antibody (1:1,000; Watabe-Uchida et al., 2006). For Western blots depicted in Fig. S1 (A and B), tissues prepared from the V-SVZ and RMSp as well as the OB and RMSa of P10 and P45 CD1 mice were snap-frozen in liquid nitrogen, sonicated in 1% SDS buffer, and subjected to Western blot analysis with rabbit polyclonal anti-DOCK7 antibody (1:1,000; Watabe-Uchida et al., 2006) and rabbit monoclonal anti-GAPDH antibody (1:1,000; 5174; Cell Signaling Technology) as a loading control. For the Western blot depicted in Fig. S2 C, lysates prepared from HeLa

cells or from the V-SVZ and RMSp of P10 CD1 mice (see above) were subjected to Western blot analysis with rabbit polyclonal anti-DOCK7 antibody (1:1,000; Watabe-Uchida et al., 2006), rabbit monoclonal anti-TACC3 antibody (1:1,000; ab134154; Abcam), and rabbit monoclonal anti-GAPDH antibody (1:1,000; 5174; Cell Signaling Technology) as a loading control. For Western blots depicted in Fig. S3 (A–C), cultured cortical neurons (A) and Neuro-2a cells (B and C) expressing indicated constructs were homogenized in RIPA buffer and subjected to Western blot analysis with rabbit polyclonal anti-p116^{Rip} antibody (1:1,000; NBP1-81035; Novus Biologicals; A) or mouse monoclonal anti-HA antibody (1:1,000; 11583816001; Sigma-Aldrich; B and C), and mouse monoclonal anti–γ-tubulin antibody (1:10,000; T6557; Sigma-Aldrich; A) or mouse monoclonal anti–α-tubulin antibody (1:2,000; T5168; Sigma-Aldrich; B and C) as a loading control.

Rac1-GTP pulldown assay

To assay Rac1 activity, GST-PBD pulldown assays were performed as described previously (Govek et al., 2004; Yu et al., 2015) using HEK293T cells expressing indicated constructs. In brief, cell lysates were prepared from HEK293T cells and incubated with GST-PBD–coupled Glutathione Sepharose beads in cell lysis buffer (50 mM Tris, pH 7.5, 10 mM $MgCl_2$, 0.5 M NaCl, and 0.05% NP-40). The beads were washed four times with wash buffer (25 mM Tris, pH 7.5, 30 mM $MgCl_2$, and 40 mM NaCl), and proteins bound on beads were examined by immunoblot analysis with anti-Rac1 mouse monoclonal antibody (1:500; ARC03; Cytoskeleton).

Immunohistochemistry

For making brain sections, mice (CD1) were deeply anesthetized with isoflurane and perfused transcardially with 4% PFA in PBS. Brains were removed and postfixed in 4% PFA in PBS at 4°C overnight. After postfixation, brains were incubated in (a) PBS for 12 h, (b) 10% sucrose in PBS for 1 h, and (c) 20% sucrose in PBS overnight, embedded in OCT compound, and then cut into 50-µm-thick coronal sections on a CM3050S cryostat (Leica Biosystems; Fig. 1, B and C; Fig. 5, C and G; and Fig. S1, D and E). For Figs. 2 B, 4 B, 6 A, 7 A, S3 D, and S4 B, brains were incubated in 30% sucrose in PBS overnight after overnight postfixation in 4% PFA in PBS, embedded in 4% agarose, and subsequently sectioned into 50-µm-thick sagittal sections using a vibratome (VT1000S; Leica Biosystems). Brain sections were blocked and permeabilized with 1% BSA and 0.2% Triton X-100 in PBS for 30 min at RT followed by incubation with primary antibodies diluted in 1% BSA and 0.2% Triton X-100 in PBS at concentrations indicated below at 4°C overnight. The following primary antibodies were used: rabbit polyclonal anti-DOCK7 (1:500; Watabe-Uchida et al., 2006) or rabbit polyclonal Alexa Fluor 488–conjugated anti-DOCK7 (1:200; bs-11825R-A488; Bioss), chicken polyclonal antinestin (1:1,000; NES; Aves Labs), chicken polyclonal anti-GFAP (1:1,000; GFAP; Aves Labs), mouse monoclonal anti-MASH1 (1:2,000; 556604; BD), goat polyclonal anti-DCX (1:1,000; sc-8066; Santa Cruz Biotechnology, Inc.), rat monoclonal anti-BrdU (1:1,000; OBT0030; AbD Serotec), rabbit polyclonal anti-GFP (1:1,000; 598; MBL), and rabbit polyclonal anti-p116^{Rip} (1:250; NBP1-81035; Novus Biologicals). Of note, for BrdU staining, brain sections were incubated in 2 N HCl solution for 30 min at 37°C to unmask the antigen, followed by a neutralization step with 0.1 M sodium tetraborate and three washes in PBS. The secondary antibodies used were Alexa Fluor 488, 555, 594, or 647 goat or donkey anti–mouse, –rabbit, –rat, –goat, or –chicken (1:1,000; A-11008, A-11042, A-21207, A-21422, A-21432, and A-31571; Molecular Probes) and CF647 donkey anti–goat (1:1,000; 20048; Biotium). Nuclei were counterstained with DAPI in mounting medium. Imaging of brain sections was performed on a PerkinElmer spinning-disk confocal microscope controlled by Volocity software (PerkinElmer) and an ORCA-R2 charge-coupled device camera (Hamamatsu Photonics) or an LSM 780 confocal microscope with GaAsP photomultiplier tubes controlled by ZEN software (Zeiss).

Postnatal in vivo electroporation and BrdU labeling

Electroporation was performed largely as described previously (Belvindrah et al., 2011). In brief, P2–3 CD1 mouse pups were anesthetized on ice for 3–4 min, and animals were maintained on a 4°C cold pad during the entire injection procedure. Plasmid solution (2 µl of a 2.5–5 µg/µl solution) was injected manually into the right lateral ventricles using a beveled and calibrated micropipette. Five 50-ms pulses of 130 V with a 950-ms interval were then delivered with a 7-mm tweezer electrode positioned on each side of the pup's head (ECM830; BTX). After electroporation, pups were reanimated on a heating pad and returned to their mother. Brains were collected for immunohistochemical analysis or slice culture and videomicroscopy 5, 7, or 14 d after electroporation. For BrdU labeling experiments, mouse pups were electroporated at P3, and BrdU (100 mg/kg of body weight) was injected 7 d after electroporation. Animals were sacrificed 2 h after BrdU injection. All animal care protocols were approved by Cold Spring Harbor Laboratory.

Quantitative analyses of electroporated forebrain-fixed slice preparations

All quantification studies (Fig. 2, B–F; Fig. 4, B–D; Fig. 6, A–C; Fig. 7, A–C; Fig. S1 F–H; Fig. S3, D–G; and Fig. S4, B and C) were performed on transfected cells located within the V-SVZ–RMS–OB pathway in fixed brain slices. To score images, the GFP channel was first judged independently, followed by judgments of the other markers. A total of two to five brain sections were analyzed per animal by taking up to three 10–20-µm z stack images to cover the electroporated V-SVZ and/or RMS and OB of each sagittal section with a 4× or 20× objective (CFI Plan Apochromat Lambda 4× 0.2 NA or CFI Plan Apochromat VC 20× 0.75 NA; Nikon) and comparing them with equivalent sections in the corresponding control groups. Quantification of the distribution of EGFP$^+$ transfected cells along the V-SVZ–RMS–OB pathway was performed on single optical sections by quantifying all EGFP$^+$ cells in the V-SVZ, RMSp, RMSa, and OB and then dividing by the total number of EGFP$^+$ cells. The number of BrdU$^+$ and/or nestin$^+$ or DCX$^+$ transfected (EGFP$^+$) cells in the V-SVZ was quantified and calculated as the percentage of total or nestin$^+$ or DCX$^+$ transfected cells. The length of the neuroblasts' LP was measured as the distance from the base of the cell body at the LP/cell body junction to the tip of the LP. All quantifications were conducted blindly using Volocity software.

Time-lapse imaging of migrating neuroblasts in brain slices

Time-lapse imaging of migrating neuroblasts in acute mouse brain slices was performed largely as described previously (Sonego et al., 2013). In brief, mouse pups at P2–3 were electroporated with indicated constructs together with a tdTomato-expressing plasmid, and animals were sacrificed 5 d after electroporation. The electroporated brains were isolated and immediately placed in precooled Gey's balanced salt solution (136.89 mM NaCl, 1.5 mM $CaCl_2$, 4.96 mM KCl, 0.22 mM KH_2PO_4, 0.97 mM $MgCl_2 \cdot 6\,H_2O$, 0.28 mM $MgSO_4 \cdot 7\,H_2O$, 2.7 mM $NaHCO_3$, 0.85 mM NaH_2PO_4, 5.55 mM D-glucose, pH 7.4, bubbled with 95% O_2, and 5% CO_2), and right hemispheres were sliced into 300-µm-thick sagittal sections with a vibratome (VT1200; Leica Biosystems). Slices containing fluorescently labeled neuroblasts along the entire RMS were chosen and transferred to a membrane insert (30 mm; 0.4 µm pore size; Millicell) placed in a glass-bottomed microwell dish (MatTek Corporation) containing slice culture medium (DMEM supplemented with 5% FCS, 0.5% glucose, 2 mM GlutaMAX, 2% B27 supplement, 10 mM

Hepes, pH 7.4, 100 U/ml penicillin, and 100 µg/ml streptomycin), and were incubated for ∼1 h at 37°C in a 5% CO_2 incubator. Subsequently, the slices were observed with an inverted spinning-disk confocal microscope equipped with an environmental chamber (5% CO_2 at 37°C; PerkinElmer). Confocal z stack images (taken every 4 µm over an interval of 100–150 µm) of tdTomato$^+$ transfected cells in the lower vertical arm of the RMSp were taken every 4 min for 4 h using a 20× long-distance objective (CFI Super Plan Fluor extra-long working distance 20× 0.45 NA, Nikon). Videos were acquired and analyzed using Volocity software (Improvision). Neuroblasts were selected for tracking if they could be followed during the entire duration of the video. Migrated distance, displacement, velocity, and branching events/hour were quantified using Volocity software.

Time-lapse imaging of migrating neuroblasts in Matrigel cultures

Dissociated neuroblasts from V-SVZ tissue dissected from P1–3 mice were transfected with indicated constructs together with a vector expressing either EGFP-P2A-PACT-mKO1 or mEGFP–Lifeact-7–P2A-PACT-mKO1 using the Amaxa nucleofector system. The transfected cells were suspended in neurobasal medium containing 10% FBS and reaggregated, and the aggregates were embedded in 66.7% Matrigel/neurobasal medium (containing 2% B27 and 2 mM GlutaMAX) 2 d after nucleofection and then cultured for 6–15 h (Falenta et al., 2013). Time-lapse images were captured at 3-min intervals for 2 h using an LSM 780 confocal microscope and a Plan Apochromat 63× 1.40 NA oil objective (ZEISS). At every time point, confocal images at multiple consecutive z planes (8–15 levels) at 1.8-µm step intervals were collected and projected to the horizontal plane for subsequent analyses. During image acquisition, neuroblasts in Matrigel culture were maintained at 37°C and 5% CO_2 in a humidified chamber (ZEISS) attached to the LSM 780 confocal microscope. Images were analyzed and quantified with ZEN software.

Immunostaining of V-SVZ neuroblasts in 2D and 3D culture

Dissociated neuroblasts from V-SVZ tissue were dissected from P1–3 mice and plated on coverslips or embedded in Matrigel as described in the Cell culture and transfection section. The following primary antibodies were used: rabbit polyclonal anti-GFP (1:1,000; 598; MBL), mouse monoclonal anti–βIII-tubulin/Tuj1 (1:2,000; MMS-435P; Covance), rabbit polyclonal anti-DOCK7 Alexa Fluor 488–conjugated (1:200; bs-11825R-A488; Bioss), goat polyclonal anti-DCX (1:1,000; sc-8066; Santa Cruz Biotechnology, Inc.), and rabbit polyclonal anti-p116^{Rip} (1:250; NBP1-81035; Novus Biologicals). The secondary antibodies used were Alexa Fluor 488 and 555 goat anti–rabbit and –mouse (1:1,000; A-11008 and A-21425; Molecular Probes) and CF647 donkey anti–goat (1:1,000; 20048; Biotium). Nuclei were counterstained with DAPI in mounting medium. Fluorescent images were acquired using an LSM 780 confocal microscope with a Plan Apochromat 40× 1.40 NA or 63× 1.40 NA oil objective lens (ZEISS).

Statistical analysis

All data are presented as means ± SEM. Comparison of two groups was made using unpaired two-tailed Student's *t* tests. For comparison of more than two groups, one-way or two-way ANOVAs were performed, followed by Dunnett's post hoc tests for evaluation of pairwise group differences. Data distribution was assumed to be normal, but this was not formally tested. A p-value <0.05 was considered to be statistically significant. The analyses were performed using Prism 6.0 software (GraphPad Software).

Online supplemental material

Fig. S1 shows additional DOCK7 expression data and its effect on the proliferation of V-SVZ stem/progenitor cells and neuroblasts. Fig. S2 shows biochemical characterization of DOCK7-DHR2 mutants, branching phenotypes of migrating V-SVZ neuroblasts expressing Dock7#2 shRNA together with DOCK7ΔDHR2 or DOCK7ΔR2, and expression data for TACC3 in the V-SVZ/RMSp. Fig. S3 shows additional data concerning the effect of p116^{Rip} knockdown on neuroblast migration. Fig. S4 shows the effect of ectopic expression of the R2 fragment of DOCK7 in neuroblasts, mapping of the minimum p116^{Rip} binding region of DOCK7 and the branching phenotypes of migrating V-SVZ neuroblasts expressing Dock7#2 shRNA together with DOCK7Δp116^{Rip}. Fig. S5 shows the requirement of DOCK7/p116^{Rip} signaling for V-SVZ neuroblast migration in Matrigel cultures. Videos 1–7 show migratory properties of V-SVZ neuroblasts expressing scr#1 shRNA (Video 1), Dock7#2 shRNA (Video 2), Dock7#2 shRNA$^+$DOCK7 (Video 3), Dock7#2 shRNA$^+$DOCK7ΔDHR2 (Video 4), Dock7#2 shRNA$^+$DOCK7ΔR2 (Video 5), p116^{Rip}#1 shRNA (Video 6), and Dock7#2 shRNA$^+$DOCK7Δp116^{Rip} (Video 7) in acute brain slices. Videos 8–12 show centrosomal and somal movements during nucleokinesis in control neuroblasts (Videos 8 and 10), neuroblasts expressing p116^{Rip}#1 shRNA or Dock7#2 shRNA together with DOCK7Δp116^{Rip} (Videos 9 and 11), or neuroblasts expressing Dock7#2 shRNA (Video 12) in Matrigel cultures.

Acknowledgments

We thank members of the Van Aelst laboratory and E.-E. Govek for discussions and/or critical reading of the manuscript. We thank K. John for YTH screening and S. Hearn and N. El-Amine for technical assistance with microscopy. We also thank W. Moolenaar, D. Solecki, and A. Sakakibara for reagents.

This work was supported by National Institutes of Health grants R01MH082808 and R01NS082266 to L. Van Aelst. S. Nakamuta was supported by the Uehara Memorial Foundation, and C.-L. Wang was supported by National Institutes of Health grant T32 CA 148056-1.

The authors declare no competing financial interests.

Author contributions: S. Nakamuta, Y.-T. Yang, C.-L. Wang, N. B. Gallo, and L. Van Aelst conceived and/or designed the project. S. Nakamuta, Y.-T. Yang, C.-L. Wang, N. B. Gallo, J.-R. Yu, and Y. Tai performed all the experiments. L. Van Aelst wrote the paper.

Submitted: 24 April 2017
Revised: 1 September 2017
Accepted: 15 September 2017

References

Alvarez-Buylla, A., and J.M. Garcia-Verdugo. 2002. Neurogenesis in adult subventricular zone. *J. Neurosci.* 22:629–634.

Anton, E.S., H.T. Ghashghaei, J.L. Weber, C. McCann, T.M. Fischer, I.D. Cheung, M. Gassmann, A. Messing, R. Klein, M.H. Schwab, et al. 2004. Receptor tyrosine kinase ErbB4 modulates neuroblast migration and placement in the adult forebrain. *Nat. Neurosci.* 7:1319–1328. https://doi.org/10.1038/nn1345

Arenkiel, B.R. 2010. Adult neurogenesis supports short-term olfactory memory. *J. Neurophysiol.* 103:2935–2937. https://doi.org/10.1152/jn.00179.2010

Bellion, A., J.P. Baudoin, C. Alvarez, M. Bornens, and C. Métin. 2005. Nucleokinesis in tangentially migrating neurons comprises two alternating phases: forward migration of the Golgi/centrosome associated with centrosome splitting and myosin contraction at the rear. *J. Neurosci.* 25:5691–5699. https://doi.org/10.1523/JNEUROSCI.1030-05.2005

Belluzzi, O., M. Benedusi, J. Ackman, and J.J. LoTurco. 2003. Electrophysiological differentiation of new neurons in the olfactory bulb. *J. Neurosci.* 23:10411–10418.

Belvindrah, R., A. Nissant, and P.M. Lledo. 2011. Abnormal neuronal migration changes the fate of developing neurons in the postnatal olfactory bulb. *J. Neurosci.* 31:7551–7562. https://doi.org/10.1523/JNEUROSCI.6716-10.2011

Carleton, A., L.T. Petreanu, R. Lansford, A. Alvarez-Buylla, and P.M. Lledo. 2003. Becoming a new neuron in the adult olfactory bulb. *Nat. Neurosci.* 6:507–518.

Chesler, A.T., C.E. Le Pichon, J.H. Brann, R.C. Araneda, D.J. Zou, and S. Firestein. 2008. Selective gene expression by postnatal electroporation during olfactory interneuron neurogenesis. *PLoS One.* 3:e1517. https://doi.org/10.1371/journal.pone.0001517

Codega, P., V. Silva-Vargas, A. Paul, A.R. Maldonado-Soto, A.M. Deleo, E. Pastrana, and F. Doetsch. 2014. Prospective identification and purification of quiescent adult neural stem cells from their in vivo niche. *Neuron.* 82:545–559. https://doi.org/10.1016/j.neuron.2014.02.039

Cooper, J.A. 2013. Mechanisms of cell migration in the nervous system. *J. Cell Biol.* 202:725–734. https://doi.org/10.1083/jcb.201305021

Doetsch, F., and A. Alvarez-Buylla. 1996. Network of tangential pathways for neuronal migration in adult mammalian brain. *Proc. Natl. Acad. Sci. USA.* 93:14895–14900. https://doi.org/10.1073/pnas.93.25.14895

Evsyukova, I., C. Plestant, and E.S. Anton. 2013. Integrative mechanisms of oriented neuronal migration in the developing brain. *Annu. Rev. Cell Dev. Biol.* 29:299–353. https://doi.org/10.1146/annurev-cellbio-101512-122400

Falenta, K., S. Gajendra, M. Sonego, P. Doherty, and G. Lalli. 2013. Nucleofection of rodent neuroblasts to study neuroblast migration in vitro. *J. Vis. Exp.* 81:e50989.

Fishell, G., and M.E. Hatten. 1991. Astrotactin provides a receptor system for CNS neuronal migration. *Development.* 113:755–765.

Fuentealba, L.C., K. Obernier, and A. Alvarez-Buylla. 2012. Adult neural stem cells bridge their niche. *Cell Stem Cell.* 10:698–708. https://doi.org/10.1016/j.stem.2012.05.012

Gadea, G., and A. Blangy. 2014. Dock-family exchange factors in cell migration and disease. *Eur. J. Cell Biol.* 93:466–477. https://doi.org/10.1016/j.ejcb.2014.06.003

Gebbink, M.F., O. Kranenburg, M. Poland, F.P. van Horck, B. Houssa, and W.H. Moolenaar. 1997. Identification of a novel, putative Rho-specific GDP/GTP exchange factor and a RhoA-binding protein: control of neuronal morphology. *J. Cell Biol.* 137:1603–1613. (published correction appears in *J. Cell Biol.* 2001. 153:?1339) https://doi.org/10.1083/jcb.137.7.1603

Ghashghaei, H.T., C. Lai, and E.S. Anton. 2007. Neuronal migration in the adult brain: are we there yet? *Nat. Rev. Neurosci.* 8:141–151. https://doi.org/10.1038/nrn2074

Godin, J.D., N. Thomas, S. Laguesse, L. Malinouskaya, P. Close, O. Malaise, A. Purnelle, O. Raineteau, K. Campbell, M. Fero, et al. 2012. p27(Kip1) is a microtubule-associated protein that promotes microtubule polymerization during neuron migration. *Dev. Cell.* 23:729–744. https://doi.org/10.1016/j.devcel.2012.08.006

Govek, E.E., S.E. Newey, C.J. Akerman, J.R. Cross, L. Van der Veken, and L. Van Aelst. 2004. The X-linked mental retardation protein oligophrenin-1 is required for dendritic spine morphogenesis. *Nat. Neurosci.* 7:364–372. https://doi.org/10.1038/nn1210

Govek, E.E., M.E. Hatten, and L. Van Aelst. 2011. The role of Rho GTPase proteins in CNS neuronal migration. *Dev. Neurobiol.* 71:528–553. https://doi.org/10.1002/dneu.20850

Hatten, M.E. 2002. New directions in neuronal migration. *Science.* 297:1660–1663. https://doi.org/10.1126/science.1074572

He, M., Z.H. Zhang, C.B. Guan, D. Xia, and X.B. Yuan. 2010. Leading tip drives soma translocation via forward F-actin flow during neuronal migration. *J. Neurosci.* 30:10885–10898. https://doi.org/10.1523/JNEUROSCI.0240-10.2010

Hirota, Y., T. Ohshima, N. Kaneko, M. Ikeda, T. Iwasato, A.B. Kulkarni, K. Mikoshiba, H. Okano, and K. Sawamoto. 2007. Cyclin-dependent kinase 5 is required for control of neuroblast migration in the postnatal subventricular zone. *J. Neurosci.* 27:12829–12838. https://doi.org/10.1523/JNEUROSCI.1014-07.2007

James, R., Y. Kim, P.E. Hockberger, and F.G. Szele. 2011. Subventricular zone cell migration: lessons from quantitative two-photon microscopy. *Front. Neurosci.* 5:30. https://doi.org/10.3389/fnins.2011.00030

Kaneko, N., O. Marín, M. Koike, Y. Hirota, Y. Uchiyama, J.Y. Wu, Q. Lu, M. Tessier-Lavigne, A. Alvarez-Buylla, H. Okano, et al. 2010. New neurons clear the path of astrocytic processes for their rapid migration in the adult brain. *Neuron.* 67:213–223. https://doi.org/10.1016/j.neuron.2010.06.018

Kappeler, C., Y. Saillour, J.P. Baudoin, F.P. Tuy, C. Alvarez, C. Houbron, P. Gaspar, G. Hamard, J. Chelly, C. Métin, and F. Francis. 2006. Branching and nucleokinesis defects in migrating interneurons derived from doublecortin knockout mice. *Hum. Mol. Genet.* 15:1387–1400. https://doi.org/10.1093/hmg/ddl062

Kempermann, G., H. Song, and F.H. Gage. 2015. Neurogenesis in the Adult Hippocampus. *Cold Spring Harb. Perspect. Biol.* 7:a018812. https://doi.org/10.1101/cshperspect.a018812

Kim, Y., I. Comte, G. Szabo, P. Hockberger, and F.G. Szele. 2009. Adult mouse subventricular zone stem and progenitor cells are sessile and epidermal growth factor receptor negatively regulates neuroblast migration. *PLoS One.* 4:e8122. https://doi.org/10.1371/journal.pone.0008122

Koga, Y., and M. Ikebe. 2005. p116Rip decreases myosin II phosphorylation by activating myosin light chain phosphatase and by inactivating RhoA. *J. Biol. Chem.* 280:4983–4991. https://doi.org/10.1074/jbc.M410909200

Koizumi, H., H. Higginbotham, T. Poon, T. Tanaka, B.C. Brinkman, and J.G. Gleeson. 2006. Doublecortin maintains bipolar shape and nuclear translocation during migration in the adult forebrain. *Nat. Neurosci.* 9:779–786. https://doi.org/10.1038/nn1704

Komuro, H., and P. Rakic. 1998. Distinct modes of neuronal migration in different domains of developing cerebellar cortex. *J. Neurosci.* 18:1478–1490.

Lalli, G. 2014. Extracellular signals controlling neuroblast migration in the postnatal brain. *Adv. Exp. Med. Biol.* 800:149–180. https://doi.org/10.1007/978-94-007-7687-6_9

Laurin, M., and J.F. Côté. 2014. Insights into the biological functions of Dock family guanine nucleotide exchange factors. *Genes Dev.* 28:533–547. https://doi.org/10.1101/gad.236349.113

Lazarini, F., and P.M. Lledo. 2011. Is adult neurogenesis essential for olfaction? *Trends Neurosci.* 34:20–30. https://doi.org/10.1016/j.tins.2010.09.006

Leong, S.Y., and A.M. Turnley. 2011. Regulation of adult neural precursor cell migration. *Neurochem. Int.* 59:382–393. https://doi.org/10.1016/j.neuint.2010.12.024

Leong, S.Y., C.H. Faux, A. Turbic, K.J. Dixon, and A.M. Turnley. 2011. The Rho kinase pathway regulates mouse adult neural precursor cell migration. *Stem Cells.* 29:332–343. https://doi.org/10.1002/stem.577

Lim, D.A., and A. Alvarez-Buylla. 2016. The Adult Ventricular-Subventricular Zone (V-SVZ) and Olfactory Bulb (OB) Neurogenesis. *Cold Spring Harb. Perspect. Biol.* 8:a018820. https://doi.org/10.1101/cshperspect.a018820

Lois, C., and A. Alvarez-Buylla. 1994. Long-distance neuronal migration in the adult mammalian brain. *Science.* 264:1145–1148. https://doi.org/10.1126/science.8178174

Lois, C., J.M. García-Verdugo, and A. Alvarez-Buylla. 1996. Chain migration of neuronal precursors. *Science.* 271:978–981. https://doi.org/10.1126/science.271.5251.978

Luskin, M.B. 1993. Restricted proliferation and migration of postnatally generated neurons derived from the forebrain subventricular zone. *Neuron.* 11:173–189. https://doi.org/10.1016/0896-6273(93)90281-U

Marín, O., and J.L. Rubenstein. 2003. Cell migration in the forebrain. *Annu. Rev. Neurosci.* 26:441–483. https://doi.org/10.1146/annurev.neuro.26.041002.131058

Marín, O., M. Valiente, X. Ge, and L.H. Tsai. 2010. Guiding neuronal cell migrations. *Cold Spring Harb. Perspect. Biol.* 2:a001834. https://doi.org/10.1101/cshperspect.a001834

Martini, F.J., and M. Valdeolmillos. 2010. Actomyosin contraction at the cell rear drives nuclear translocation in migrating cortical interneurons. *J. Neurosci.* 30:8660–8670. https://doi.org/10.1523/JNEUROSCI.1962-10.2010

Mejia-Gervacio, S., K. Murray, T. Sapir, R. Belvindrah, O. Reiner, and P.M. Lledo. 2012. MARK2/Par-1 guides the directionality of neuroblasts migrating to the olfactory bulb. *Mol. Cell. Neurosci.* 49:97–103. https://doi.org/10.1016/j.mcn.2011.10.006

Merkle, F.T., L.C. Fuentealba, T.A. Sanders, L. Magno, N. Kessaris, and A. Alvarez-Buylla. 2014. Adult neural stem cells in distinct microdomains generate previously unknown interneuron types. *Nat. Neurosci.* 17:207–214. https://doi.org/10.1038/nn.3610

Métin, C., R.B. Vallee, P. Rakic, and P.G. Bhide. 2008. Modes and mishaps of neuronal migration in the mammalian brain. *J. Neurosci.* 28:11746–11752. https://doi.org/10.1523/JNEUROSCI.3860-08.2008

Miyamoto, Y., and J. Yamauchi. 2010. Cellular signaling of Dock family proteins in neural function. *Cell. Signal.* 22:175–182. https://doi.org/10.1016/j.cellsig.2009.09.036

Mulder, J., M. Poland, M.F. Gebbink, J. Calafat, W.H. Moolenaar, and O. Kranenburg. 2003. p116Rip is a novel filamentous actin-binding protein. *J. Biol. Chem.* 278:27216–27223. https://doi.org/10.1074/jbc.M302399200

Mulder, J., A. Ariaens, D. van den Boomen, and W.H. Moolenaar. 2004. p116Rip targets myosin phosphatase to the actin cytoskeleton and is essential for RhoA/ROCK-regulated neuritogenesis. *Mol. Biol. Cell.* 15:5516–5527. https://doi.org/10.1091/mbc.E04-04-0275

Nam, S.C., Y. Kim, D. Dryanovski, A. Walker, G. Goings, K. Woolfrey, S.S. Kang, C. Chu, A. Chenn, F. Erdelyi, et al. 2007. Dynamic features of postnatal subventricular zone cell motility: a two-photon time-lapse study. *J. Comp. Neurol.* 505:190–208. https://doi.org/10.1002/cne.21473

Obernier, K., C.K. Tong, and A. Alvarez-Buylla. 2014. Restricted nature of adult neural stem cells: re-evaluation of their potential for brain repair. *Front. Neurosci.* 8:162. https://doi.org/10.3389/fnins.2014.00162

Ota, H., T. Hikita, M. Sawada, T. Nishioka, M. Matsumoto, M. Komura, A. Ohno, Y. Kamiya, T. Miyamoto, N. Asai, et al. 2014. Speed control for neuronal migration in the postnatal brain by Gmip-mediated local inactivation of RhoA. *Nat. Commun.* 5:4532. https://doi.org/10.1038/ncomms5532

Petreanu, L., and A. Alvarez-Buylla. 2002. Maturation and death of adult-born olfactory bulb granule neurons: role of olfaction. *J. Neurosci.* 22:6106–6113.

Riddick, N., K. Ohtani, and H.K. Surks. 2008. Targeting by myosin phosphatase-RhoA interacting protein mediates RhoA/ROCK regulation of myosin phosphatase. *J. Cell. Biochem.* 103:1158–1170. https://doi.org/10.1002/jcb.21488

Sailor, K.A., A.F. Schinder, and P.M. Lledo. 2017. Adult neurogenesis beyond the niche: its potential for driving brain plasticity. *Curr. Opin. Neurobiol.* 42:111–117. https://doi.org/10.1016/j.conb.2016.12.001

Sakakibara, A., T. Sato, R. Ando, N. Noguchi, M. Masaoka, and T. Miyata. 2014. Dynamics of centrosome translocation and microtubule organization in neocortical neurons during distinct modes of polarization. *Cereb. Cortex.* 24:1301–1310. https://doi.org/10.1093/cercor/bhs411

Sakamoto, M., R. Kageyama, and I. Imayoshi. 2014. The functional significance of newly born neurons integrated into olfactory bulb circuits. *Front. Neurosci.* 8:121. https://doi.org/10.3389/fnins.2014.00121

Sawada, M., and K. Sawamoto. 2013. Mechanisms of neurogenesis in the normal and injured adult brain. *Keio J. Med.* 62:13–28. https://doi.org/10.2302/kjm.2012-0005-RE

Schaar, B.T., and S.K. McConnell. 2005. Cytoskeletal coordination during neuronal migration. *Proc. Natl. Acad. Sci. USA.* 102:13652–13657. https://doi.org/10.1073/pnas.0506008102

Shinohara, R., D. Thumkeo, H. Kamijo, N. Kaneko, K. Sawamoto, K. Watanabe, H. Takebayashi, H. Kiyonari, T. Ishizaki, T. Furuyashiki, and S. Narumiya. 2012. A role for mDia, a Rho-regulated actin nucleator, in tangential migration of interneuron precursors. *Nat. Neurosci.* 15:373–380. https://doi.org/10.1038/nn.3020

Solecki, D.J., L. Model, J. Gaetz, T.M. Kapoor, and M.E. Hatten. 2004. Par6alpha signaling controls glial-guided neuronal migration. *Nat. Neurosci.* 7:1195–1203. https://doi.org/10.1038/nn1332

Solecki, D.J., N. Trivedi, E.E. Govek, R.A. Kerekes, S.S. Gleason, and M.E. Hatten. 2009. Myosin II motors and F-actin dynamics drive the coordinated movement of the centrosome and soma during CNS glial-guided neuronal migration. *Neuron.* 63:63–80. https://doi.org/10.1016/j.neuron.2009.05.028

Sonego, M., Y. Zhou, M.J. Oudin, P. Doherty, and G. Lalli. 2013. In vivo postnatal electroporation and time-lapse imaging of neuroblast migration in mouse acute brain slices. *J. Vis. Exp.* 81:50905. https://doi.org/10.3791/50905

Sonego, M., M. Oberoi, J. Stoddart, S. Gajendra, R. Hendricusdottir, F. Oozeer, D.C. Worth, C. Hobbs, B.J. Eickholt, P.R. Gordon-Weeks, et al. 2015. Drebrin regulates neuroblast migration in the postnatal mammalian brain. *PLoS One.* 10:e0126478. https://doi.org/10.1371/journal.pone.0126478

Surks, H.K., C.T. Richards, and M.E. Mendelsohn. 2003. Myosin phosphatase-Rho interacting protein. A new member of the myosin phosphatase complex that directly binds RhoA. *J. Biol. Chem.* 278:51484–51493. https://doi.org/10.1074/jbc.M305622200

Surks, H.K., N. Riddick, and K. Ohtani. 2005. M-RIP targets myosin phosphatase to stress fibers to regulate myosin light chain phosphorylation in vascular smooth muscle cells. *J. Biol. Chem.* 280:42543–42551. https://doi.org/10.1074/jbc.M506863200

Tanaka, T., F.F. Serneo, C. Higgins, M.J. Gambello, A. Wynshaw-Boris, and J.G. Gleeson. 2004. Lis1 and doublecortin function with dynein to mediate coupling of the nucleus to the centrosome in neuronal migration. *J. Cell Biol.* 165:709–721. https://doi.org/10.1083/jcb.200309025

Taverna, E., and W.B. Huttner. 2010. Neural progenitor nuclei IN motion. *Neuron.* 67:906–914. https://doi.org/10.1016/j.neuron.2010.08.027

Tielens, S., S. Huysseune, J.D. Godin, A. Chariot, B. Malgrange, and L. Nguyen. 2016. Elongator controls cortical interneuron migration by regulating actomyosin dynamics. *Cell Res.* 26:1131–1148. https://doi.org/10.1038/cr.2016.112

Tramontin, A.D., J.M. García-Verdugo, D.A. Lim, and A. Alvarez-Buylla. 2003. Postnatal development of radial glia and the ventricular zone (VZ): a continuum of the neural stem cell compartment. *Cereb. Cortex.* 13:580–587. https://doi.org/10.1093/cercor/13.6.580

Trivedi, N., and D.J. Solecki. 2011. Neuronal migration illuminated. *Cell Adhes. Migr.* 5:42–47. https://doi.org/10.4161/cam.5.1.13609

Trivedi, N., D.R. Stabley, B. Cain, D. Howell, C. Laumonnerie, J.S. Ramahi, J. Temirov, R.A. Kerekes, P.R. Gordon-Weeks, and D.J. Solecki. 2017. Drebrin-mediated microtubule-actomyosin coupling steers cerebellar granule neuron nucleokinesis and migration pathway selection. *Nat. Commun.* 8:14484. https://doi.org/10.1038/ncomms14484

Tsai, L.H., and J.G. Gleeson. 2005. Nucleokinesis in neuronal migration. *Neuron.* 46:383–388. https://doi.org/10.1016/j.neuron.2005.04.013

Tsai, J.W., K.H. Bremner, and R.B. Vallee. 2007. Dual subcellular roles for LIS1 and dynein in radial neuronal migration in live brain tissue. *Nat. Neurosci.* 10:970–979. https://doi.org/10.1038/nn1934

Van Aelst, L. 1998. Two-hybrid analysis of Ras-Raf interactions. *Methods Mol. Biol.* 84:201–222.

Wang, Y., N. Kaneko, N. Asai, A. Enomoto, M. Isotani-Sakakibara, T. Kato, M. Asai, Y. Murakumo, H. Ota, T. Hikita, et al. 2011. Girdin is an intrinsic regulator of neuroblast chain migration in the rostral migratory stream of the postnatal brain. *J. Neurosci.* 31:8109–8122. https://doi.org/10.1523/JNEUROSCI.1130-11.2011

Watabe-Uchida, M., K.A. John, J.A. Janas, S.E. Newey, and L. Van Aelst. 2006. The Rac activator DOCK7 regulates neuronal polarity through local phosphorylation of stathmin/Op18. *Neuron.* 51:727–739. https://doi.org/10.1016/j.neuron.2006.07.020

Wichterle, H., J.M. Garcia-Verdugo, and A. Alvarez-Buylla. 1997. Direct evidence for homotypic, glia-independent neuronal migration. *Neuron.* 18:779–791. https://doi.org/10.1016/S0896-6273(00)80317-7

Yang, Y.T., C.L. Wang, and L. Van Aelst. 2012. DOCK7 interacts with TACC3 to regulate interkinetic nuclear migration and cortical neurogenesis. *Nat. Neurosci.* 15:1201–1210. https://doi.org/10.1038/nn.3171

Yu, J.R., Y. Tai, Y. Jin, M.C. Hammell, J.E. Wilkinson, J.S. Roe, C.R. Vakoc, and L. Van Aelst. 2015. TGF-β/Smad signaling through DOCK4 facilitates lung adenocarcinoma metastasis. *Genes Dev.* 29:250–261. https://doi.org/10.1101/gad.248963.114